Influence of organic sulfur gas-phase sulfation on the NH_3-SCR activity of CeO_2 catalyst: the competitive adsorption and conversion of CS_2 and COS at a low hydrolysis temperature

Zhibo Xiong[1*], Zhenchang Sun[1], Jiaxing Liu[1], Yanping Du[2], Yafei Zhu[1], Fei Zhou[3], Jing Jin[1*], Qiguo Yang[1], Wei Lu[1]

1. School of Energy and Power Engineering, University of Shanghai for Science & Technology, Shanghai, 200093, China

2. School of Engineering, Lancaster University, Lancaster, LA1 4YW, UK

3. Jiangsu Guoxin Jingjiang Power Co. Ltd., Jingjiang 214500, Jiangsu, China

Abstract:

In this study, a simplified approach is proposed to realize the gas-phase sulfation of CS_2 or/and COS at the hydrolysis temperature for further facilitating the NH_3-SCR activity of CeO_2 in diverse conditions. A low-temperature oxidation conversion process for the adsorbed CS_2 or COS on cubic fluorite CeO_2 surface is developed. It is found that the gas-phase sulfation of organic CS_2 or/and COS at 50 ^oC enhances the mobility of lattice oxygen of cubic fluorite CeO_2 and the concentration of oxygen defects for the sulfated CeO_2 catalyst, but the kinds of organic COS/CS_2 can regulate the formed types and quality of sulfur-containing species on the catalyst surfaces during the gas-phase sulfation. and the formed sulfates under the gas-phase sulfation of CS_2 are more active than those of COS, and CeO_2-CS_2-50^{o}C-3h presents the best mobility of lattice oxygen, the largest concentration of adsorbed oxygen and the best NH_3-SCR activity. Furthermore, the competitive adsorption and conversion of CS_2 and COS is disadvantageous for

* Corresponding author: Zhibo Xiong, Jing Jin, Tel.: +86 21 55272320, Email addresses: xzb412@usst.edu.cn (Z.Xiong), alicejin001@163.com (J. Jin)

the formation of oxygen vacancies on the catalyst surfaces compared to single CS_2 or COS. However, the long-time durability testing coupling re-cycle experiments can optimize the oxygen vacancy defects and increase the concentration of chemisorbed oxygen of the sulfated CeO_2-CS_2+COS-50°C-24h catalyst via optimizing the oxidization of sulfur element to sulfur oxides or/and sulfates, thereby improves its NH_3-SCR activity. And the sulfated CeO_2 catalyst by the gas-phase sulfation of organic COS+CS_2 presents a good stability for NH_3-SCR reaction. This study specifies a novel approach to simplify the gas-phase sulfation process of CeO_2 catalyst, which is valuable in promotion of the NH_3-SCR activity of CeO_2 and reduction of cost in experimental procedures.

Keywords: NH_3-SCR, CeO_2, Organic COS/CS_2, Low-temperature gas-phase sulfation, Competitive adsorption and conversion

1. Introduction

As the major compounds of organic sulfur, carbonyl sulfide (COS) and carbon disulfide (CS_2) widely present in petrochemical energy sources, including coal, natural gas and water gas [1,2], which have cytotoxic effects on the human central nervous system (CNS) and also can corrode the production equipment, resulting in the poisoning/deactivation of catalysts and the depressed utilization rate of the industrial by-product resources [3-5]. Similar to carbon dioxide (CO_2), COS and CS_2 with the linear molecular configurations are stable at room temperature and difficult to be removed via the traditional adsorption method applied for SO_2 and H_2S [6-8]. Therefore, the catalytic hydrolysis has been promoted to reduce COS/CS_2 due to the low energy consumption, simple operation and few side reactions. The main hydrolysis reactions are listed as follows [2,5]:

$$CS_2 + H_2O \rightarrow \mathrm{COS} + H_2S \quad (1)$$

$$COS + H_2O \rightarrow CO_2 + H_2S \quad (2)$$

$$H_2S + O_2 \rightarrow H_2O + \mathrm{S}/SO_4^{2-} \quad (3)$$

It is clear that the basic sites of catalysts are the active centers for the hydrolysis reaction, which are divided into the weak (-OH groups)/medium basic sites (metal-oxygen pairs, Al-O, Zn-O, Ti-O, Ce-O, etc.) and the strong basic sites (O^{2-} ions), respectively. It was reported in previous studies that CS_2 and COS were firstly adsorbed on the catalyst surfaces through ion coupling, and interacted with the surface -OH groups and metal-oxygen pairs to produce the intermediate product thiocarbonate ($HSCO_2^-$), which subsequently reacted with the basic sites to form H_2S and CO_2. Finally, H_2S was oxidized to elemental sulfur or/and sulfate species by-products by the strong basic sites (O^{2-}, etc.) and partial weak/medium basic sites on the catalyst surfaces [9-12]. Therefore, the catalytic hydrolysis of COS/CS_2 could induce the formation of sulfate species on the catalyst surfaces, thus deactivating and poisoning the hydrolysis activity of the Al_2O_3/TiO_2 alkali catalysts, especially under the condition of oxygen in flue gas. However, the doping of cerium oxide effectively inhibited the sulfation of surface alkaline active sites due to its stronger combination ability with sulfate species, and improved the anti-O_2 poisoning of the hydrolysis alkali catalysts [13-17].

Due to the unique 4f electronic structure, cerium dioxide (CeO_2) presents an excellent oxygen storage capacity (OSC) and a redox ability via the redox cycle of Ce^{4+}/Ce^{3+}, and has attracted a widespread attention in developing a replaced non-vanadium-based catalyst for selective catalytic reduction of NO_x with NH_3 (NH_3-SCR) [18-21]. Unfortunately, single CeO_2 exhibits a bad NH_3-SCR activity owing to the poor surface acidity and the side reactions at high-temperatures, which needs to be optimized. Interestingly, the sulfation has been used to improve the NH_3-SCR activity of CeO_2 by enhancing its surface acidity. Previous studies had confirmed that the gas-phase sulfation

of SO_2 at 300 °C and below could cause sulfate species formed on cubic fluorite CeO_2 surfaces, and enhanced its Brønsted acid sites on the basis of retaining Lewis acid sites, thus accelerated the adsorption and activation of NH_3 on the cerium-base catalyst surfaces [22-26]. For example, Xie et al. [27] had investigated the influence of SO_2 sulfation time on regulating the formed sulfate species on the CeO_2 catalyst surface and its NH_3-SCR activity, and found that under the sulfation of SO_2 at 150 °C, the enhancement of sulfation time increased the formed amount of sulfate on the catalyst surfaces, thus gradually improved the NH_3-SCR activity of CeO_2 due to the increased Brønsted acid sites, exhibiting a higher adsorption rate of NH_3 species than Lewis acid sites. This phenomenon had also been confirmed by the research on the sulfated Ce/TiO_2 catalyst [22]. Furthermore, the sulfation temperature could adjust the formed types of sulfate species. Zhang et al. [28] found that the enhancement of sulfation temperature converted the surface sulfates to bulk-like sulfates and even bulk sulfates in the CeO_2 catalyst, which promoted the NH_3-SCR reaction of CeO_2 below 300 °C. Comparatively, the higher temperature bulk-like and/or bulk sulfate species hindered the synergistic catalytic effect between surface sulfates and bulk CeO_2, which depressed the promotional effect of sulfation. It should be mentioned that the organic COS/CS_2 had also been used to optimize the NH_3-SCR activity of CeO_2 in our previous research. We found that compared to the traditional inorganic SO_2, the reductive COS/CS_2 presented better promotional effect on the catalytic performance of NO_x reduction over CeO_2, and the gas-phase sulfation of CS_2 at 300 °C induced more Ce^{4+} to reduce to Ce^{3+} and generated more surface defects owing to its stronger reducibility than SO_2, thus leading to more oxygen defects and chemisorbed oxygen formed on the CeO_2 surfaces [29]. Therefore, the organic sulfur, including COS and CS_2, presented stronger optimized effect on the NH_3-SCR activity of cerium-based catalyst. However, the gas-phase sulfation of

89 COS/CS_2 at low temperatures on the NH_3-SCR activity of CeO_2 has been little reported, so it is
90 critical to examine the characteristics of its influence on catalysis at different hydrolysis
91 temperatures.

92 Actually, the temperature of flue gas emitted from industrial steel, glass or/and boiler typically
93 ranges from 70-150 ^oC, and the developed alkali catalysts have also been expected to reduce organic
94 sulfur via the low-temperature hydrolysis method, which is beneficial to lower cost by avoiding the
95 reheating of flue gas and reducing the formation of S or/and SO_4^{2-} on the catalyst surfaces to prevent
96 poisoning [16,30,31]. Meanwhile, the gas-phase sulfation temperature also affects the NH_3-SCR
97 activity of cerium-based catalysts, and higher sulfation temperature might induce the formation of
98 thermostable bulk sulfates, which deactivated the activity of cerium-based catalysts through
99 destroying the redox conversion between Ce^{4+} and Ce^{3+} [32,33]. However, the gas-phase sulfation
100 at a low temperature could inhibit the formation of bulk sulfate species on the surfaces of CeO_2
101 catalyst, facilitating the propagation of the redox reaction. Furthermore, the adsorbed surface sulfate
102 species optimized its acid sites and active species, thereby increased the NH_3-SCR activity of CeO_2
103 [27,34]. Therefore, as the additive to improve the anti-O_2 poisoning of alkali catalysts for the
104 hydrolysis of organic sulfur, CeO_2 presents a stronger combination ability with sulfate species
105 compared to the surface alkaline active sites, thus the sulfated CeO_2 catalysts by organic COS/CS_2
106 at low-temperatures can exhibit a good NH_3-SCR activity due to the formation of active surface
107 sulfate species. Nevertheless, organic COS or CS_2 might show different adsorption and conversion
108 characteristics on the CeO_2 surfaces under the hydrolysis temperature, affecting the NH_3-SCR
109 activity of the sulfated CeO_2 catalyst attributed to the diversely formed surface sulfate species and
110 active sites.

In this study, organic CS_2 or/and COS were used to improve the NH_3-SCR activity of CeO_2 by the gas-phase sulfation at their low temperature hydrolysis temperatures. It is found that the types of organic sulfur influence the promotional effect of their gas-phase sulfation on the NH_3-SCR activity of CeO_2, and the gas-phase sulfation of reductive CS_2 at 50 °C shows the best promotional effect. Meanwhile, because the co-existence of CS_2 and COS reduces the catalyst activity due to their competitive adsorption and conversion, the synergistic effect of organic sulfur types on the physicochemical properties of the gas-phase sulfated CeO_2 catalyst at 50 °C was specifically examined. The characterization results are further validated by comparing with theoretical calculations based on density functional theory (DFT) using the Dmol^3 module in the Material Studio calculation software. This simple gas-phase sulfation strategy can be generally extended to other supported metal oxide catalysts to improve their catalytic performance of NO_x reduction.

2. Experimental

2.1. Synthesis of CeO_2

Based on our previous researches [29,35], a one-pot hydrothermal method was used to obtain CeO_2 with cerium nitrate ($Ce(NO_3)_3 \cdot 6H_2O$, AR), ammonium bicarbonate (NH_4HCO_3, AR) and hydrogen peroxide (30% H_2O_2, AR) as the precursor, precipitant and oxidant, respectively. Firstly, 0.005 mol $Ce(NO_3)_3 \cdot 6H_2O$ was dissolved in 50 mL distilled water under vigorous stirring for 2 hours until a clear solution is formed. Then, 0.02 mol NH_4HCO_3 was added into the above solution under the continuous stirring, and a white precipitation is immediately generated. Subsequently, the above white suspension promptly becomes orange accompanied with the release of bubbles when 9 mL H_2O_2(10 mol/L) was dropped into it. After being vigorous stirred for 3 h, the obtained solution was carefully transferred into a 100 mL Teflon-lined autoclave and then heated at 200 °C for 24 h.

After the hydrothermal treatment, the autoclave was cooled down quickly to room temperature, and then the obtained precipitant was filtered and thoroughly washed several times by distilled water and absolute ethanol. After being dried at 80 ^{o}C for 12 h, the sample was calcined at 400 ^{o}C for 5 h in a temperature-programmed muffle furnace.

2.2. Synthesis of sulfated CeO_2

The gas-phase sulfation of CeO_2 was carried out in a tube furnace under a simulated sulfur-containing atmosphere at 300 ^{o}C or the hydrolysis temperature of organic sulfur [36,37]. The types and concentrations of organic sulfur were specified as follow: CS_2/COS/CS_2+COS (the CS_2/COS molar ratio of 3:7), the concentration of S element is 200 ppm, and the total flow rate was 500 mL/min with N_2 (99.999 vol.%) as balance. In the experiments, the pretreated samples were recorded as CeO_2-CS_2-t-h, CeO_2-COS-t-h and CeO_2-CS_2+COS-t-h, where t and h represent the temperature and duration of sulfation, respectively. For example, CeO_2-CS_2-50^{o}C-3h presented the catalyst treated by the gas-phase sulfation of CS_2 at 50 ^{o}C for 3 h. Furthermore, the sulfated CeO_2-CS_2+COS-50^{o}C-24h catalysts after the long-time stability test coupling re-cycle experiments and the secondary re-calcination at 400 ^{o}C for 5 h are denoted as CeO_2-CS_2+COS-50^{o}C-24h-CT and CeO_2-CS_2+COS-50^{o}C-24h-SC, respectively. All samples were screened by 40-60 meshes for the activity evaluation.

2.3. Catalytic activity test

The NH_3-SCR catalytic performance at a temperature range of 150~400 °C was tested in a fixed bed micro-reactor by using 0.45 g catalyst (40~60 mesh). The corresponding gas hourly space velocity (GHSV) is 200,000 mL/(g·h) under the total flow rate of 1500 mL/min for the simulated flue gas, comprising 600 ppm NH_3, 600 ppm NO, 5 vol.% O_2 and balance gas 99.999 vol.% N_2.

After the reaction system reaches a stable state, the activity test data was recorded to avoid the effect of gas adsorption on the catalyst. The concentrations of O_2 and NO_x at inlet and outlet were continuously monitored by T-350 flue gas analyzer (Testo, Germany), and the NO_x conversion rate (η) was calculated according to the following formula: $\eta = (1-[NO_x]_{out}/[NO_x]_{in})\times 100\%$, where $[NO_x]_{in}$ and $[NO_x]_{out}$ represented the inlet and outlet concentrations of gaseous NO_x (NO and NO_2), respectively.

2.4. Catalyst characterizations

N_2 adsorption-desorption, Scanning electron microscopy (SEM), Transmission electron microscopy (TEM), High-resolution transmission electron microscopy (HR-TEM) and Energy-dispersive X-ray spectroscopy (EDS), X-ray diffraction (XRD), Raman spectra, Fourier transform infrared spectra (FTIR), X-ray photoelectron spectroscopy (XPS), H_2 temperature programmed reduction (H_2-TPR) and infrared spectroscopy with pyridine desorption (Py-IR) experiments were carried out to investigate the physical-chemical properties of the samples [29,35], and the detailed testing process were given in supporting information (SI).

Furthermore, Thermogravimetric Analysis (TGA) and Derivative Thermogravimetry (DTG) were performed in a α-Al_2O_3 crucible using PerkinElmer STA6000. Thermogravimetric curves were recorded at a heating rate of 10 °C/min from 30 to 900 °C in nitrogen atmosphere. Thermogravimetric-Mass spectrometry analysis (TG-MS) was used to qualitatively analyze the volatile components released during the heating up of the sulfated CeO_2 catalyst. The TG-MS measurement of the samples was performed in a α-Al_2O_3 crucible using a TG-MS system (PerkinElmer STA6000 thermal analyzer and STA409 PC-QMS403C mass spectrometry). TG-MS curves were recorded from 50 to 900 °C at a heating rate of 10 °C/min in an argon atmosphere (40

177 mL/min). In the characterization, The TG-MS diagram was analyzed for evaluating the amount of
178 evolved gas products during the thermal decomposition of a single compound.

179 ## 2.5. Computational method

180 The crystal plane (111) of the synthesized CeO_2 catalyst by the one-pot hydrothermal method
181 was regarded as the surface model to obtain the adsorption energies of COS or CS_2 over the sample
182 in this study [35]. All simulation calculations were performed using the $Dmol^3$ module in the
183 Material Studio calculation software [38], and the GGA/PBE functional in density functional theory
184 was employed in approximating the electron-related exchange energy [3,39]. The Hubbard
185 parameter U = 5 eV was used to correct the Coulomb interaction of Ce to more accurately describe
186 the valence electron structure of Ce 4f orbital. The density functional semi-core pseudopotential
187 method was adopted for the core electrons of Ce, while the all-electron method was utilized for the
188 core electrons of H, C, O, and S atoms. The double-value plus d-function (DND) basis set 4.4
189 version and a 5.8 Å orbital cutoff value were applied in the simulation. The energy, gradient, and
190 displacement convergence tolerances were 1.0×10^{-5} Ha, 2.0×10^{-3} Ha/Å, and 5.0×10^{-3} Å, respectively.
191 In the condition that at least two of these criteria are fulfilled, self-consistent field convergence can
192 be assumed [40]. Theoretically, the unit cell of CeO_2 belongs to the orthorhombic system, with a
193 symmetrical space group of FM-3M. A 3×3×3 Monkhorst-Pack K-point grid was utilized to
194 optimize the bulk structure of CeO_2. The optimized configuration for the structure is shown in Fig.
195 S1(A). The calculated lattice parameter for the structure is a=b=c= 5.488 Å, and compared with the
196 lattice parameter 5.400 Å obtained from the experimental test, the error is less than 2 %, which is
197 within the acceptable range. Thus, it can be considered that the parameters set in this study are
198 reliable. In the model, a periodic CeO_2 (111) surface model with nine atomic layers arranged in a

(4×4) supercell was constructed and a 15 Å vacuum layer was used to prevent the influence of the underlying atoms on the surface calculation. The Monkhorst-Pack grid with a k point of 2×2×1 was sampled in the first Brillouin zone. The optimized CeO_2 (111) model is shown in Fig. S1(B).

3. Results and discussion

3.1. Catalytic performances

Compared to the traditional inorganic SO_2, after the gas-phase sulfation at 300 °C for 3 h, the organic CS_2 with a stronger reducibility presented a better promotional effect on the NH_3-SCR activity of CeO_2. This is because more Ce^{3+} and oxygen defects were induced, causing more chemisorbed oxygen formation on the catalyst surfaces. In addition, the gas-phase sulfation of CS_2 also facilitated the formation of sulfate species, augmenting the abundance and strength of both Brønsted acid sites and low-temperature Lewis acid sites on the catalyst surfaces [29]. Actually, the low-temperature hydrolysis coupled chemical absorption method had been confirmed to be an effective mean for the removal of organic CS_2/COS based on the alkali catalysts, and cerium oxide had also been discovered as an excellent additive to improve their anti-O_2 poisoning via depressing the sulfation of components [40,41]. Moreover, previous research indicated that the sulfation temperature could affect the promotional effect of SO_2 gas-phase sulfation. Therefore, the influence of sulfation temperature on the NH_3-SCR activity of CeO_2 were studied for organic CS_2, as shown in Fig. S2(A). Interestingly, compared to the sulfation at 300 °C, the low-temperature gas-phase sulfation of reductive CS_2 further increases the catalytic performance of NO_x reduction over CeO_2, especially at its hydrolysis temperature of 50 °C. The better promotional effect of low-temperature gas-phase sulfation on the NH_3-SCR activity of cerium oxide catalyst for organic sulfur COS was validated, as presented in Fig. S2(B). Therefore, it is clear that the gas-phase sulfation of CS_2/COS

presents stronger enhancement on the NH_3-SCR activity of CeO_2 under their hydrolysis temperatures, which implies that there might exist a mutual promotion effect of organic sulfur low-temperature hydrolysis and NO_x reduction over the cerium-based catalyst.

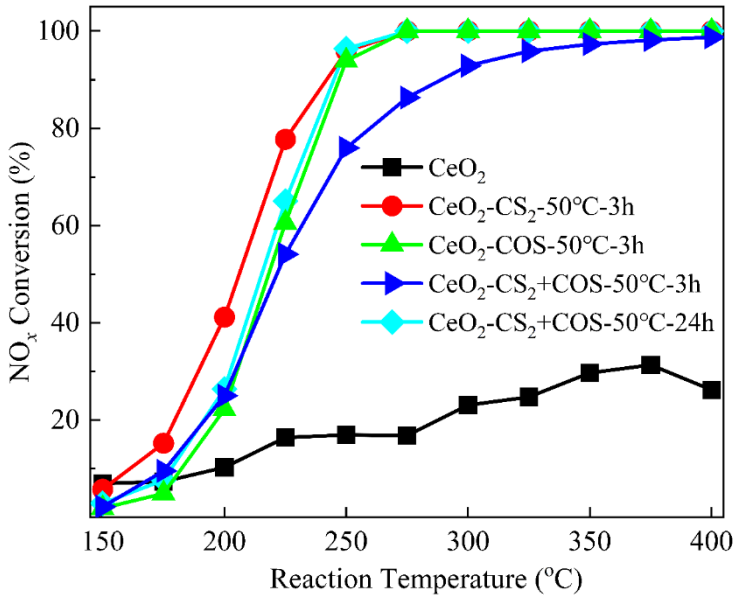

Fig. 1. Influence of competitive sulfation for organic CS_2 and COS on the NH_3-SCR activity of CeO_2 catalyst at low-temperature. The concentrations of CS_2 or/and COS during the gas-phase sulfation: CS_2 or COS or CS_2+COS (the CS_2/COS molar ratio of 3:7) with the total amount of S element being 200 ppm.

Fig. S2(C) and (D) show the influence of CS_2/COS sulfation duration at 50 °C on the activity of CeO_2, respectively. It is found that the NO_x reduction over catalysts firstly increases and then decreases, and the suitable sulfate duration is 3 h for CS_2 under the gas-phase sulfation conditions. However, CeO_2-COS-50°C-24h presents better catalytic performance of NO_x reduction than CeO_2-COS-50°C-3h. These demonstrate that the sulfation or transformation of CS_2 and COS over CeO_2 might be different at the hydrolysis temperature of 50 °C. For featuring the processes, the promotional effect of CS_2+COS composite components gas-phase sulfation on the NH_3-SCR activity of CeO_2 at 50 °C for 3 and 24 h was investigated, as shown in Fig. 1. In consideration of the proportion of each component of blast furnace gas and the experimental simulation conditions, the

concentrations of CS_2 and COS in the simulated flue gas component were set to be 3:7 with the total amount of S element being 200 ppm [39,42,43]. From Fig. 1, it can be found that CeO_2-CS_2-50°C-3h and CeO_2-COS-50°C-3h present better NH_3-SCR activity than CeO_2-CS_2+COS-50°C-3h, which indicates that the co-existence of CS_2 and COS decreases the promotional effect of their gas-phase sulfation on the NO_x reduction over CeO_2. Interestingly, the enhancement of sulfation duration from 3 to 24 h increases the NH_3-SCR activity of CeO_2-CS_2+COS-50°C-3h. Comparatively, CeO_2-CS_2+COS-50°C-24h presents similar catalytic performance to CeO_2-COS-50°C-3h. This indicates that there might exist a competitive adsorption and conversion of CS_2 and COS over cubic fluorite CeO_2 under the hydrolysis temperature of 50 °C [4,44]. In order to better evaluate the catalytic performance of the CeO_2-CS_2+COS-50°C-24h catalyst treated by organic sulfur at low-temperatures, the NO_x conversions and N_2 selectivity over the reported Ce-based catalysts modified by the gas-phase sulfation are summarized and shown in Table 1. As seen in the Table 1, the N_2 selectivity of the sulfated catalysts is greater than 95% in the whole active temperature window, which indicates that the gas-phase sulfated catalysts we used in the research have excellent N_2 selectivity. It is also shown in the table that CeO_2-CS_2+COS-50°C-24h exhibits excellent NH_3-SCR activity under the high GHSV of 200,000 mL/(g·h). Therefore, it is evident that the gas-phase sulfation of organic sulfur is an effective measure to optimize the selectivity and the NH_3-SCR activity of cerium-based catalyst simultaneously.

Table 1. The summaries of catalytic activity and N_2 selectivity over the Ce-based catalysts modified by the gas-phase sulfation.

Catalysts	Gas-phase sulfation	NO_x conversion	Temperature window (°C)	Temperature window (°C) (N_2	GHSV/MHSV	Reference

	temperature (°C)	(%) at 250 °C	(X_{NO}>90%)	Selectivity>95%)		
CeO_2-rod-SO_2	350	50-60	350-425	200-500	180,000 mL/(g·h)	[24]
S-C6Z4	200	80-90	250-350	100-400	96,000 mL/(g·h)	[45]
S-CeO_2-72h	150	80-90	350-500	150-550	60,000 mL/(g·h)	[46]
S-Ce/Ti	300	80-90	275-325	150-400	120,000 mL/(g·h)	[47]
SO_4^{2-}/CeO_2-VS	100	60-70	275-300	100-300	60,000 mL/(g·h)	[48]
S-FCT	250	70-80	270-420	150-420	30,000 mL/(g·h)	[49]
CeO_2-CS_2+COS-50°C-24h	50	96	250-400	/	200,000 mL/(g·h)	In this paper

257

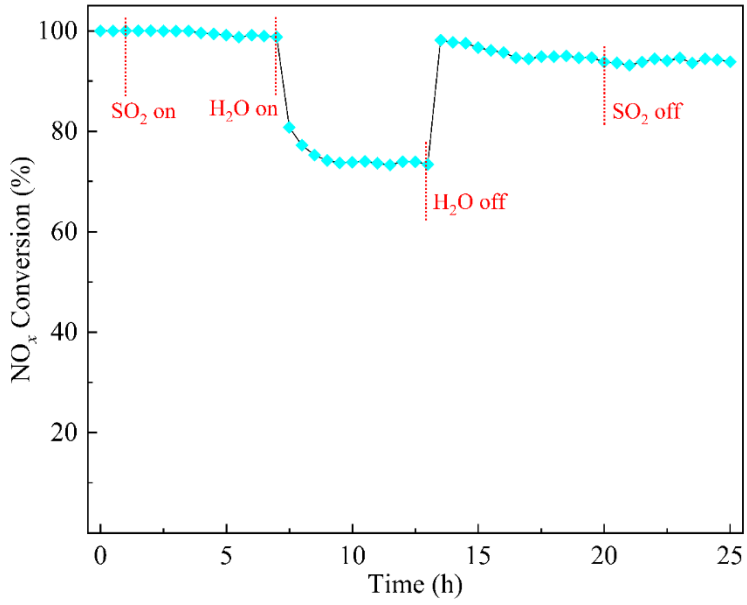

258

259 **Fig. 2.** The effect of H_2O and SO_2 on the NO_x conversion of CeO_2-CS_2+COS-50°C-24h catalyst. (Reaction

260 Conditions: reaction temperature 300 °C, [NO] = [NH_3] = 600 ppm, [O_2] = 5.0 vol.%, [SO_2] = 100 ppm (when

261 used), [H_2O] = 10.0 vol.% (when used), N_2 balance, the total rate=1500 mL8/min, GHSV=200,000 mL/(g·h))

262 Due to the poisoning of H_2O or/and SO_2 on the NH_3-SCR activity of catalyst, the influence of

263 H_2O or/and SO_2 on the activity of the sulfated CeO_2-CS_2+COS-50°C-24h catalyst was investigated

264 at 300 °C herein, as shown in Fig. 2. The NO_x conversion of CeO_2-CS_2+COS-50°C-24h catalyst at

265 300 °C maintains at almost 100% when 100 ppm SO_2 is introduced into the simulated flue gas,

indicating that the sulfated CeO_2-CS_2+COS-50°C-24h catalyst presents excellent anti-SO_2 poisoning. Meanwhile, the further introduction of 10.0 vol.% H_2O results in a rapid decrease of NO_x conversion to 73% and then remains stable, mainly attributed to the competitive adsorption of H_2O and NH_3 on the catalyst surfaces [50]. After the removal of H_2O, the NO_x conversion quickly recovers to 95% and then gradually decrease. Furthermore, the NO_x conversion doesn't return to the initial value when SO_2 was also cut off. The results show that the deactivation caused by SO_2 and H_2O on CeO_2-CS_2+COS-50°C-24h catalyst can be divided into the reversible deactivation and the irreversible deactivation. The reversible deactivation was mainly attributed to the competitive adsorption of SO_2 and H_2O on the active sites of the catalyst with the reaction gas, while the irreversible deactivation is attributed to the sulfate species formed by SO_2 on the catalyst surface covering the active sites and inhibiting the adsorption and conversion of reactants on the catalyst surface [26,51].

3.2. Catalyst characterization

3.2.1. Pore structure and surface morphology analysis

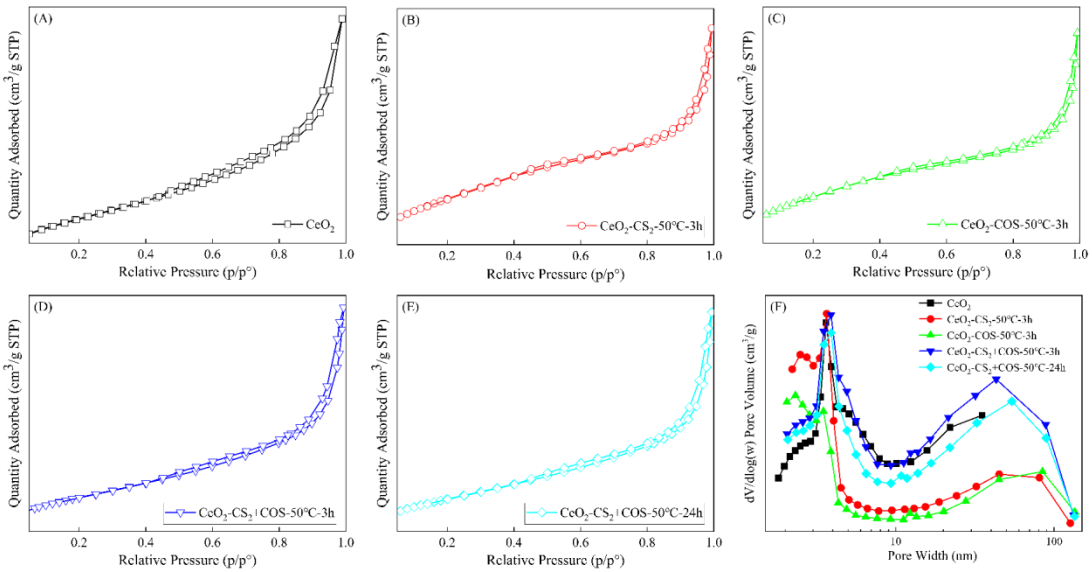

Fig. 3. The N_2 adsorption-desorption isotherms (A-E) and the pore size distributions (F) of catalysts.

Fig. 3 gives the N_2 adsorption-desorption isotherms and pore size distributions of the samples. It can be seen that the gas-phase sulfation of organic sulfur at 50 °C shows no effect on the adsorption-desorption isotherm of CeO_2, and all catalysts present type IV of N_2 adsorption-desorption isotherms with H3 hysteresis loops [52,53]. In addition, the adsorption capacity of N_2 displays significant enhancement at a higher pressure in the range of 0.9~1.0 and the stable adsorption plateau is not observed, demonstrating the mesoporous and macroporous structure due to the accumulation of nanoparticles [9,54]. The pore size distributions in Fig. 3(F) indicate that the gas-phase sulfation of CS_2 or COS at 50 °C enlarges the mesopores smaller than 3 nm, but decreases the mesopores larger than 3 nm. And CeO_2-CS_2-50°C-3h and CeO_2-COS-50°C-3h present the concentrated mesopores at 2~4 nm. However, the gas-phase sulfation at 50 °C under the co-existence of COS and CS_2 exhibits no effect on the pore size distribution of CeO_2, even if the sulfation duration is up to 24 h. This indicates that the co-existence of COS and CS_2 might indeed affect their adsorption and conversion on cubic fluorite CeO_2 surfaces. The calculated data in Table 2 demonstrates that the gas-phase sulfation of CS_2 or COS at 50 °C decreases the BET surface area and the pore volume of CeO_2, but the co-existence of COS and CS_2 enlarges its BET surface area when the gas-phase sulfation duration is 3 h. Furthermore, CeO_2-CS_2+COS-50°C-24h still exhibits larger BET surface area and pore volume than CeO_2-CS_2-50°C-3h and CeO_2-COS-50°C-3h. Generally, larger specific surface area is closely related to a higher NH_3-SCR activity of catalysts. However, it is noteworthy that CeO_2-CS_2-50°C-3h with the smallest surface area presents the best catalytic performance of NO_x reduction as shown in Fig. 1. Hence, it can be inferred that the specific surface area may not be the determinant factor on affecting the NH_3-SCR activity of the cerium oxide catalyst sulfated by organic COS or/and CS_2 at low-temperatures.

To further investigate the influence of organic sulfur gas-phase sulfation on the morphology of CeO_2 at their hydrolysis temperature of 50 °C, SEM was utilized and the results are given in Fig. 4 and Fig. S3. Our previous study had pointed out that the as-prepared CeO_2 via the one-pot hydrothermal method exhibited disorderly dispersed particles with some agglomeration due to the accumulation of nanoparticles [35]. Meanwhile, the gas-phase sulfation of COS or/and CS_2 at 50 °C for 3 h slightly weakened the agglomeration and crystallinity of CeO_2, which might be mainly attributed to the formation and deposition of sulphate species or/and sulfur element on the catalyst surfaces. It is seen that the enhancement of sulfation duration to 24 h increases the agglomeration of surface nanoparticles compared to CeO_2-CS_2+COS-50°C-3h. This might result from larger sulfate species or/and sulfur element deposited on the catalyst surfaces due to the long-term sulfation.

Table 2. The physical structural parameters of the as-synthesized catalysts.

Samples	BET surface area [a] (m^2/g)	Pore volume [b] (cm^3/g)	Pore diameter [c] (nm)
CeO_2	119.62	0.199	6.44
CeO_2-CS_2-50°C-3h	108.27	0.168	6.14
CeO_2-COS-50°C-3h	108.28	0.150	6.44
CeO_2-CS_2+COS-50°C-3h	127.86	0.280	8.34
CeO_2-CS_2+COS-50°C-24h	111.54	0.239	8.18

[a] BET surface area

[b] BJH desorption pore volume

[c] BJH desorption pore diameter

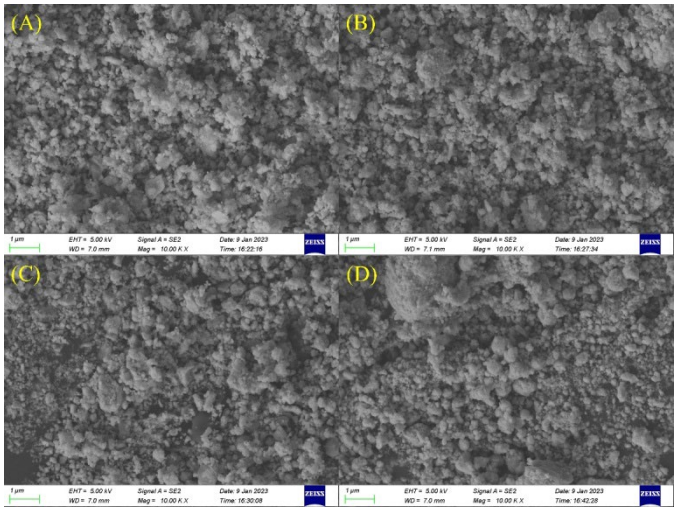

Fig. 4. The SEM images of (A) CeO_2-CS_2-50°C-3h, (B) CeO_2-COS-50°C-3h, (C) CeO_2-CS_2+COS-50°C-3h and (D) CeO_2-CS_2+COS-50°C-24h catalysts.

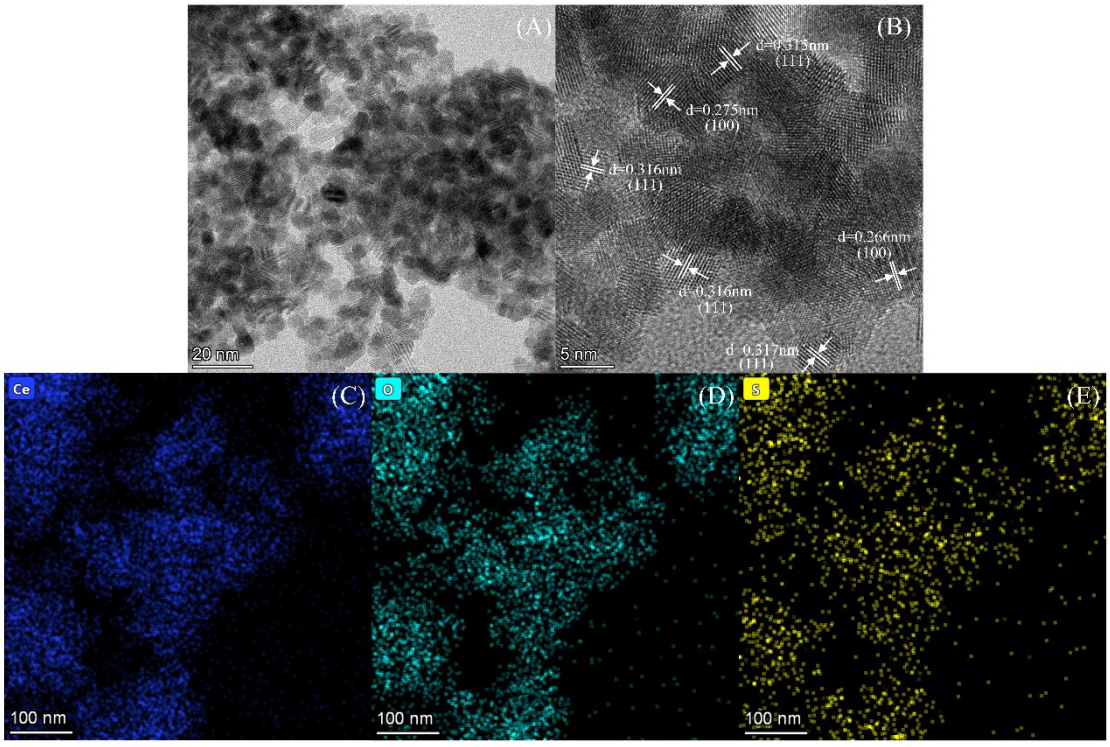

Fig. 5. The TEM/HR-TEM images and the elemental mapping images of the as-prepared CeO_2-CS_2+COS-50°C-24h catalyst.

The TEM/HR-TEM analysis was used to further elucidate more detailed morphological information of CeO_2-CS_2+COS-50°C-24h catalyst, and the results are shown in Fig. 5. According to the Fig. 5(A), it can be observed that this sulfated catalyst exhibits nanoparticle morphology and

agglomeration, which is consistent with the findings of SEM. Furthermore, the HR-TEM image in Fig. 5(B) indicates that the interplanar spacings on the surface are about 0.316 nm and 0.275 nm, corresponding to the lattice fringes of the (111) and (100) facets of cubic fluorite CeO_2, respectively. However, our previous research found that the as-synthesized CeO_2 catalyst by the one-pot hydrothermal method exposed the (111) crystal plane [35]. This indicates that the gas-phase sulfation of CS_2 and COS at 50 °C for 24 h might result in a transformation of partial (111) facet to (100) facet of cubic fluorite CeO_2 on the catalyst surfaces. It should be mentioned that CeO_2-CS_2+COS-50ºC-24h presents a uniform distribution of Ce, O, and S elements across the catalyst surfaces in a consistent distribution trend according to the elemental mapping images in Fig. 5(C-E). This demonstrates that the gas-phase sulfation of organic CS_2+COS contributes to resulting in the formation of high dispersive sulfates and sulfur on the surface of CeO_2 catalyst, which might be beneficial to the redox capacity and surface acidity of catalyst.

3.2.2. XRD

The X-ray diffraction (XRD) patterns of samples were measured and it was found that the low-temperature gas-phase sulfation of organic COS or/and CS_2 could effectively reduce the intensity of cubic fluorite CeO_2 crystal in cerium oxide catalyst. Thus, in order to clearly reveal the effect of organic sulfur types, the XRD patterns of the sulfated catalysts and the standard cards of the corresponding sulfur-containing species are presented in Fig. 6 with the XRD of CeO_2 and its standard card (#34-0394) shown in Fig. S4 for comparisons. CeO_2 presents high crystalline cubic fluorite structures. After the gas-phase sulfation of organic COS or/and CS_2 at 50 ºC, there still exists the main cubic fluorite CeO_2 for the sulfated catalysts. However, a new broad diffraction peak appears at 10~30 º, which might be attributed to sulfates or/and sulfur elemental deposition.

According to the enlarged XRD patterns at 10~35 ° in Fig. 6(B), the wider peak of the sulfated catalysts at a lower scanning angle (15~26 °) corresponds to sulfates ($Ce_2(SO_4)_3·2H_2O$ #37-0762, $Ce(SO_4)_2·4H_2O$ #24-1250 and $Ce_2(SO_4)_3·(OH)_2·4H_2O$, #24-1216) and sulfur compounds [55,56]. Sun et al. [57] found that the low-temperature oxidation of H_2S could bring a broad diffraction peak of sulfur elements at approximately 25 ° formed in the nitrogen-rich mesoporous carbon catalyst. Meanwhile, in our previous study, the gas-phase sulfation of CS_2 at 300 ºC could not promote a new diffraction peak formed at 10~30 ° [29]. This indicates that the gas-phase sulfation of organic COS/CS_2 under their hydrolysis temperature of 50 ºC contributes to promoting the formation of sulfate and sulfur compounds than those at 300 ºC. It should be mentioned that CeO_2-CS_2+COS-50ºC-3h presents the similar bread diffraction peak to CeO_2-CS_2-50ºC-3h at 15~26 °, while the other two catalysts exhibit a stronger and more concentrated peak at this angle. This indicates that competitive adsorption and conversion of CS_2 and COS over CeO_2 again. When the gas-phase sulfation duration is 3 h for the coexistence of CS_2+COS, CS_2 might play a leading role in the formation of sulfur-containing species on the catalyst surfaces compared to COS. However, the enhancement of sulfation duration from 3 h to 24 h might increase the adsorption and conversion of COS on the catalyst surfaces, and CeO_2-CS_2+COS-50ºC-24h presents the similar bread diffraction peak to CeO_2-COS-50ºC-3h at 15~26 °. It should be mentioned that according to the results in Fig.1, CeO_2-COS-50ºC-3h and CeO_2-CS_2+COS-50ºC-24h also exhibit similar catalytic performance of NO_x reduction. This demonstrates that the formed types and quality of sulfur-containing species might play an important role on the NH_3-SCR activity of the sulfated CeO_2 catalysts, which can be regulated by the kinds of organic COS/CS_2 during the gas-phase sulfation at 50 ºC.

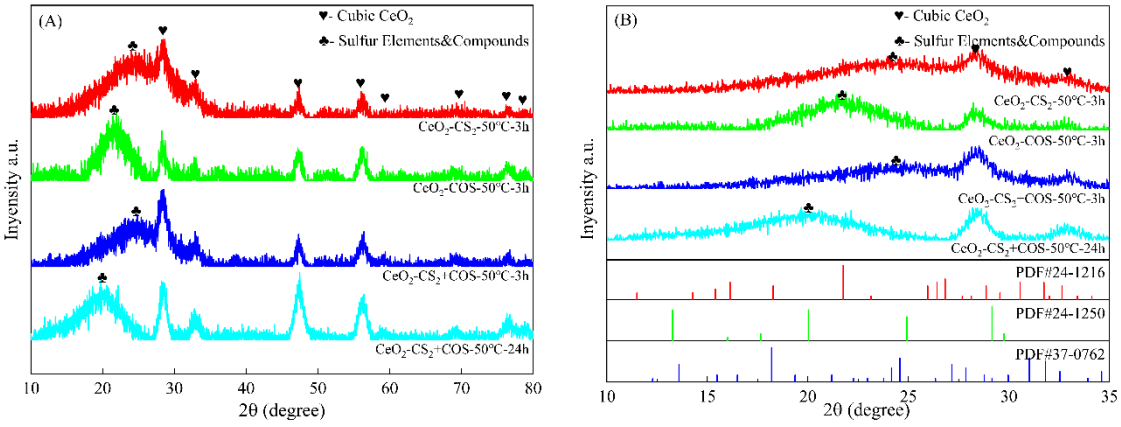

Fig. 6. The XRD patterns (A) and the locally enlarged XRD (10~35 °) (B) of catalysts.

3.2.3. Raman

Raman spectroscopy was employed to further examine the structural properties of the CeO_2 catalysts treated by organic COS or/and CS_2 at the hydrolysis temperature of 50 °C. According to the results in Fig. 7(A), three Raman spectra peaks can be observed for all catalysts. Among them, the band at 464 cm^{-1} corresponds to the F_{2g} symmetric vibration of cubic fluorite CeO_2, resulting from the symmetric breathing mode of O atoms around the Ce^{4+} cation of cubic fluorite CeO_2 [25,58]. Furthermore, as shown in Fig. 7(B), the gas-phase sulfation of organic COS or/and CS_2 makes this peak shift from 464 cm^{-1} to 461 cm^{-1}, which can be attributed to the enhancement of oxygen vacancies and Ce^{3+} cations due to the reduction of cubic fluorite CeO_2. This is due to the increase of the unit parameters of CeO_2 and reduction of its bond force constant, thus resulting in the improvement of NH_3-SCR activity [59,60].

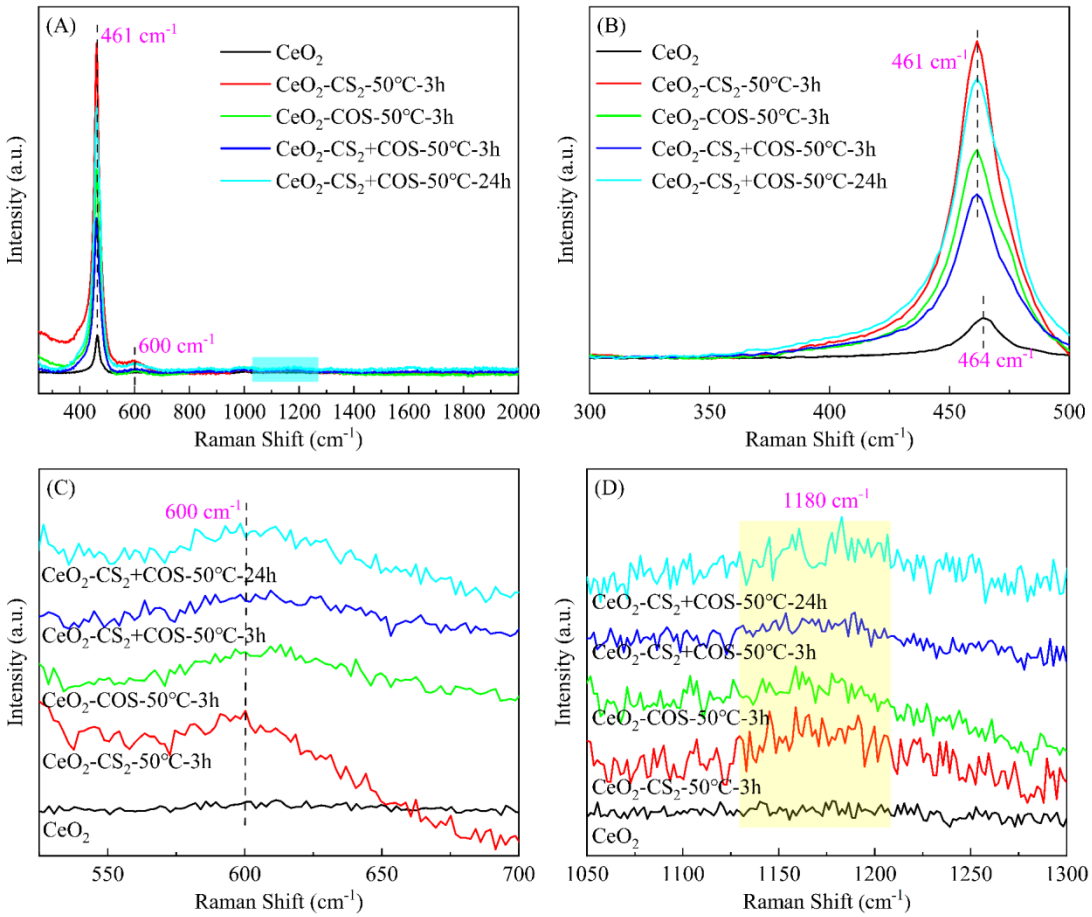

Fig. 7. The Raman spectra of CeO_2, CeO_2-CS_2-50°C-3h, CeO_2-COS-50°C-3h, CeO_2-CS_2+COS-50°C-3h and CeO_2-CS_2+COS-50°C-24h catalysts: (A) overall view (B~D) locally enlarged view.

It should be mentioned that the relative intensity of the Raman peak at 461 or 464 cm^{-1} for all catalysts decreases as follows: CeO_2-CS_2-50°C-3h > CeO_2-CS_2+COS-50°C-24h > CeO_2-COS-50°C-3h > CeO_2-CS_2+COS-50°C-3h > CeO_2, demonstrating that the reduction of Ce^{4+} to Ce^{3+} in cubic fluorite CeO_2 is closely related to the reducibility of CS_2 and COS even if the gas-phase sulfation was carried out at 50 °C. And reductive CS_2 presents a stronger reduction of Ce^{4+} to Ce^{3+} than COS, thus the replacement of partial CS_2 by COS decreases its ability of reduction. Interestingly, the co-existence of COS and CS_2 presents the worst reducibility of cubic fluorite CeO_2, but the enhancement of sulfation time up to 24 h could improve this reducibility. These indicate that there exists a competitive adsorption and conversion of CS_2 and COS over CeO_2 under the hydrolysis

395 temperature of 50 °C for the coexistence of COS+CS_2. As illustrated in Fig. 7 (C) and (D), the bands
396 at 600 cm^{-1} and 1180 cm^{-1} can be attributed to the characteristic peaks of surface oxygen defects,
397 which are related to the intrinsic Vo (oxygen vacancy) formation during $Ce^{4+} \rightarrow Ce^{3+}$ reaction [50,61].
398 The adsorbed organic COS or/and CS_2 could react with the oxygen-containing functional groups (-
399 OH, O^{2-}, O_2^{2-}, etc.) on CeO_2 surface to form sulfate species and elemental sulfur during the gas-
400 phase sulfation process [15,56]. As a result, partial Ce-O bond of cubic fluorite CeO_2 might be
401 destroyed, leading to the improvement of Ce^{3+} ions and oxygen vacancies. The latter is considered
402 to accelerate the conversion frequency between chemisorbed oxygen and lattice oxygen during the
403 converting of Ce^{4+}/Ce^{3+}, which is beneficial to the oxidization of NO to NO_2, thus increasing the
404 NH_3-SCR activity via the 'fast SCR' reaction [62-64]. Therefore, the concentrations of oxygen
405 vacancies or defects for all catalysts were obtained by calculating the relative peak intensity ratio of
406 $(I_{600}+I_{1180})/I_{461}$. As depicted in Fig. S5, the gas-phase sulfation of CS_2 or/and COS at 50 °C enhances
407 the generation of relative oxygen vacancies on CeO_2 surface. Specifically, CeO_2-CS_2-50°C-3h
408 exhibits nearly twice the amount of relative oxygen vacancies of the CeO_2 catalyst, but the co-
409 existence of CS_2 and COS depresses their promotional effect on the formation of oxygen vacancies
410 even if the sulfation time is up to 24 h. This demonstrates that the improvement of Ce^{4+} to Ce^{3+} does
411 not bring the corresponding oxygen vacancies on the catalyst surfaces, and the competitive
412 adsorption and conversion of CS_2 and COS is disadvantageous for the formation of oxygen
413 vacancies compared to single CS_2 or COS.

414 **3.2.4. XPS analysis**

415 X-ray Photoelectron Spectroscopy (XPS) tests were conducted to investigate the effect of
416 organic CS_2 or/and COS sulfation on the dispersion of elements and their relative concentrations on

CeO_2 surface. As shown in Fig. 8(A), there exist both Ce^{3+} (u' and v') and Ce^{4+} (u, u", u"', v, v", and v"') on the catalysts surfaces by fitting the XPS spectra of Ce 3d into eight characteristic peaks [65-67], but the gas-phase sulfation of organic COS or/and CS_2 at 50 °C can make the binding energy of Ce 3d XPS spectra shift to higher value, indicating the interaction between CS_2/COS and CeO_2, which reduces the electron cloud density around cerium ion and alters the chemical environment of Ce and O species [9,68]. Generally, the electron transfer process from Ce^{4+} to Ce^{3+} is useful to promote the creation of oxygen vacancies, and the presence of Ce^{3+} could boost the charge imbalance and facilitate the redox cycle between Ce^{4+} and Ce^{3+}, thus improves the catalyst activity towards oxygen molecule activation and reaction [69-71]. Therefore, the molar ratios of $Ce^{3+}/(Ce^{3+}+Ce^{4+})$ were calculated and the results are given in Table 3. It can be found that the gas-phase sulfation of organic COS or/and CS_2 at 50 °C increases the surface $Ce^{3+}/(Ce^{3+}+Ce^{4+})$ molar ratio of CeO_2, especially the gas-phase sulfation of CS_2 for 3 h. Interestingly, the co-existence of COS and CS_2 decreases the sulfation of Ce^{4+} on CeO_2 surface compared to CS_2 and COS, and CeO_2-CS_2+COS-50°C-3h presents a higher surface concentration of Ce species and a lower $Ce^{3+}/(Ce^{3+}+Ce^{4+})$ molar ratio than CeO_2-CS_2-50°C-3h and CeO_2-COS-50°C-3h. In addition, the enhancement of sulfation time up to 24 h can further decrease the concentration of Ce species on CeO_2-CS_2+COS-50°C-3h surface and enlarge its surface $Ce^{3+}/(Ce^{3+}+Ce^{4+})$ molar ratio, which is similar to the value of CeO_2-COS-50°C-3h. This regularity is consistent to the XRD results as shown in Fig. 6 and the phenomenon of long sulfation for the co-existence of COS and CS_2 might be approximate to the sample sulfated using COS at 50 °C for 3 h.

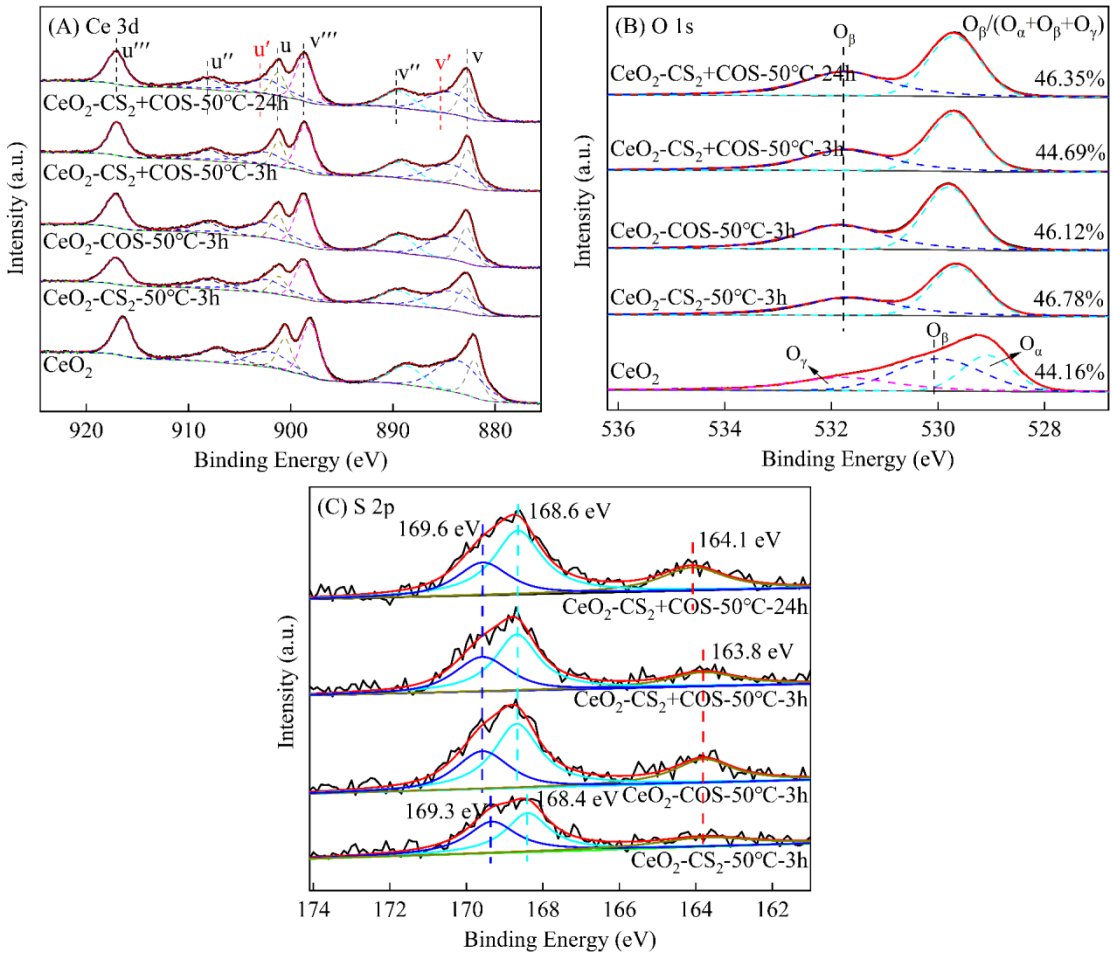

437

438 **Fig. 8.** The XPS spectra of CeO_2, CeO_2-CS_2-50°C-3h, CeO_2-COS-50°C-3h, CeO_2-CS_2+COS-50°C-3h and

439 CeO_2-CS_2+COS-50°C-24h catalysts: (A)Ce 3d, (B)O 1s, (C)S 2p.

440 **Table 3.** Surface compositions and atomic ratios of the as-prepared catalysts calculated from XPS.

Catalysts	Atomic concentrations (%)			Atomic ratios (%)		
	Ce	O	S	$Ce^{3+}/(Ce^{3+}+Ce^{4+})$	$O_\beta/(O_\alpha+O_\beta+O_\gamma)$	S^{6+}/S
CeO_2	36.16	63.84	-	31.34	44.16	-
CeO_2-CS_2-50°C-3h	31.75	64.05	4.20	36.99	46.87	78.20
CeO_2-COS-50°C-3h	31.03	63.88	5.09	35.37	46.28	76.99
CeO_2-CS_2+COS-50°C-3h	32.15	63.24	4.61	31.75	44.69	80.60
CeO_2-CS_2+COS-50°C-24h	30.74	64.18	5.08	35.27	46.35	75.95
CeO_2-CS_2+COS-50°C-24h-CT	31.55	63.59	4.86	34.92	53.46	100

Numerous studies had pointed out that the surface chemisorbed oxygen presented higher mobility than lattice oxygen, and its enlargement could facilitate the oxidation of NO to NO_2, thus increased the activity of catalyst by promoting the fast NH_3-SCR reaction [50,62]. According to the results in Fig. 8(B) and Table 3, there exist three oxygen on the catalysts surfaces, attributing to the lattice oxygen (O_α), the surface chemisorbed oxygen (O_β, such as O^{2-} and O_2^{2-}) and the lattice oxygen (O_γ) bonded to Ce_2O_3 in cubic fluorite CeO_2 located at about 529 eV, 530 eV and 531.8 eV, respectively [72-74]. The gas-phase sulfation of organic COS or/and CS_2 at 50 °C also enlarges the binding energies of O 1s and increases the molar ratio of $O_\beta/(O_\alpha+O_\beta+O_\gamma)$ on CeO_2 surface and the values of $O_\beta/(O_\alpha+O_\beta+O_\gamma)$ molar ratio decreases as follows: CeO_2-CS_2-50°C-3h > CeO_2-CS_2+COS-50°C-24h > CeO_2-COS-50°C-3h > CeO_2-CS_2+COS-50°C-3h > CeO_2, which is similar to the regulation of surface $Ce^{3+}/(Ce^{3+}+Ce^{4+})$ molar ratios. Therefore, there exists a consistency in the catalytic performance of catalysts and the surface concentrations of chemisorbed oxygen and Ce^{3+} [75].

As shown in Fig. 8(C), the gas-phase sulfation of COS or/and CS_2 at 50 °C promotes the formation of S^{6+} on CeO_2 surface according to the fitting peaks of S 2p at approximately 168~170 eV, indicating the existence of sulfate species, which is consistent with the earlier research findings [26,29]. However, different from the gas-phase sulfation effect of SO_2, another new peak emerges at 163.8±0.5 eV under the action of organic CS_2 or/and COS at 50 °C for 3 h, which is attributed to sulfur element [5,10,55]. In terms of the results of XRD, it is inferred that there exist both sulfur and sulfate species on the catalysts surfaces. Meanwhile, the types of organic sulfur can affect the formed amount of sulfur species (S) and the ratio of S^{6+}/S, and the content of S on the surface of CeO_2-COS-50°C-3h (5.09%) is higher than that of CeO_2-CS_2-50°C-3h (4.20%) while CeO_2-CS_2+COS-

463 50°C-3h has 4.61% of S on its surface. But the enhancement of sulfation time up to 24 h improves
464 the formed S amount to 5.08%. This suggests the existence of partial CS_2 can decrease the formed
465 amount of sulfur species on CeO_2-COS-50°C-3h surface, even if the sulfation time is up to 24 h. It
466 should also be mentioned that the surface concentrations of Ce, O and S are very close for CeO_2-
467 COS-50°C-3h and CeO_2-CS_2+COS-50°C-24h catalysts, and their calculated surface molar ratios of
468 $Ce^{3+}/(Ce^{3+}+Ce^{4+})$, $O_\beta/(O_\alpha+O_\beta+O_\gamma)$ and S^{6+}/S are also very close, which are consistent with the NH_3-
469 SCR activity of CeO_2-COS-50°C-3h and CeO_2-CS_2+COS-50°C-24h catalysts. This demonstrates
470 that there exists a similar degree of sulfation for cubic fluorite CeO_2 for both the sulfated CeO_2-
471 COS-50°C-3h and CeO_2-CS_2+COS-50°C-24h catalysts, and the enhancement of sulfation duration
472 from 3 h to 24 h under the co-existence of COS+CS_2 improves the adsorption and conversion of
473 COS on the catalyst surfaces. Therefore, the sulfated CeO_2-COS-50°C-3h and CeO_2-CS_2+COS-
474 50°C-24h catalysts present a similar NH_3-SCR activity.

475 **3.2.5. TG-DTG and TG-MS**

476 In order to distinguish the influence of organic sulfur types on the formed sulfur species on
477 CeO_2 surfaces, TG were conducted and the results are given in Fig. 9. As illustrated, there exist three
478 major weight loss peaks at the temperature range of 30~900 °C for all the sulfated CeO_2 catalysts.
479 Among them, the weight loss peaks observed below 200 °C and above 600 °C are attributed to the
480 desorption of physically adsorbed water/hydroxyl groups and the decomposition of metal sulfate
481 species, respectively [76,77]. In addition, the weight loss peak at 200~500 °C is primarily attributed
482 to the oxidation of sulfur to SO_2, which had been validated by TG-MS. As shown in Fig. 10, the
483 TG-MS results of CeO_2-CS_2+COS-50°C-24h at 50~900 °C demonstrate that the gas produced in the
484 first weight loss interval (below 200 °C) is H_2O (m/z=18), attributed to the desorption of physically

adsorbed water and hydroxyl groups, and only SO_2 gas (m/z=64) was detected at the second weight loss range of 200~500 °C [78,79]. This suggests that the deposited sulfur can react with the oxygen-containing functional groups on CeO_2 surface to generate SO_2. During the third weight loss range (above 600 °C), SO_2 (m/z=64) and O_2 (m/z=32) are simultaneously produced due to the decomposition of metal sulfate species as follows [80,81]:

$$Ce(SO_4)_2 \rightarrow CeO_2 + 2SO_2 \uparrow + O_2 \uparrow \quad (4)$$

$$Ce_2(SO_4)_3 \rightarrow 2CeO_2 + 3SO_2 \uparrow + O_2 \uparrow \quad (5)$$

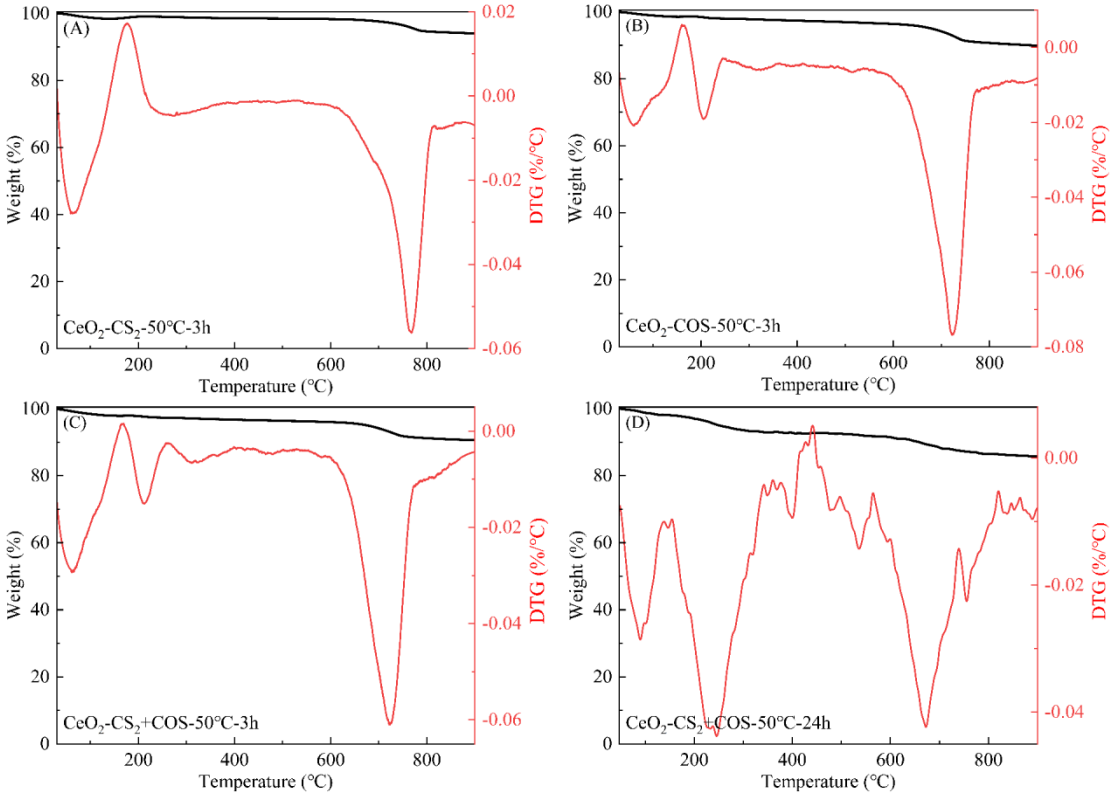

Fig. 9. The TG-DTG curves of CeO_2-CS_2-50°C-3h, CeO_2-COS-50°C-3h, CeO_2-CS_2+COS-50°C-3h and CeO_2-CS_2+COS-50°C-24h catalysts.

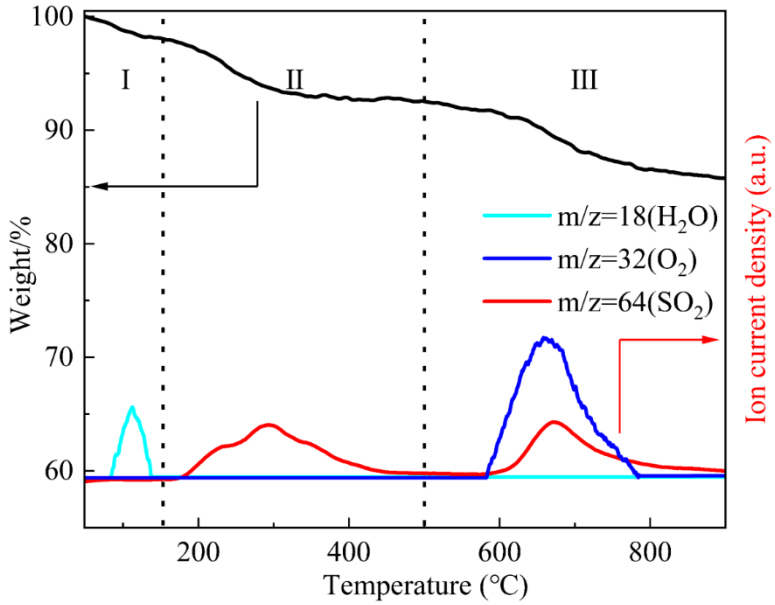

Fig. 10. The TG-MS curves of the as-prepared CeO_2-CS_2+COS-50°C-24h catalyst.

The proportions of sulfur and sulfate species formed in catalysts are calculated and shown in Table 4. Notably, the enhancement of sulfation time up to 24 h can increase the deposited amount of S, which is approximate to the sulfur content of sulfate. Furthermore, the gas-phase sulfation of COS presents a stronger promotional effect on the deposition of sulfur than that of CS_2. CeO_2-CS_2-50°C-3h shows the best low-temperature NH_3-SCR activity with the least amounts of both sulfur and sulfate, which indicates that metal sulfate species might not be the dominant role on the catalytic performance of NO_x reduction over the sulfated CeO_2 catalysts.

Table 4. The calculated proportion of sulfate species and sulfur element from the TG-DTG curves.

Samples	Sulfur element (%)	Sulfate species (%)
CeO_2-CS_2-50°C-3h	0.25	4.29
CeO_2-COS-50°C-3h	0.64	6.47
CeO_2-CS_2+COS-50°C-3h	0.54	5.44
CeO_2-CS_2+COS-50°C-24h	2.55	6.13

3.2.6. The properties of redox ability

The reduction or/and sulfur deposition during the gas-phase sulfation of organic CS_2 or/and COS at 50 °C might affect the redox properties of CeO_2, which are regarded as crucial factors on its NH_3-SCR activity. Thus, the H_2-TPR of all samples were carried out and the results are given in Fig. 11. CeO_2 displays two broad reduction peaks at 400~550 °C (region I) and 700~900 °C (region III), which are attributed to the reduction of Ce^{4+} to Ce^{3+} on the surface and subsurface and the reduction of bulk Ce^{4+} to Ce^{3+}, respectively. However, one new reduction peak emerges at 500~700 °C (region II) after the gas-phase sulfation of organic CS_2 or/and COS at 50 °C, owing to the reduction of metal sulfate species [82,83]. Yang et al. [84] had pointed out that one reduction peak located at 595 °C arose from the formed SO_4^{2-} species during the gas-phase sulfation of SO_2. Furthermore, the gas-phase sulfation of organic CS_2 at 50 °C makes the first reduction peak of CeO_2 shift to lower temperature, indicating an improvement in redox performance [22,81], while the existence of COS does not affect the peak position of this reduction peak. However, according to the results in Fig. 11(C) and Table 5, CeO_2-COS-50°C-3h presents higher temperature for the peak position and larger integral area than CeO_2-CS_2-50°C-3h at region II. Interestingly, the partial substitution of COS with CS_2 can slightly decrease these peak position temperature and integral area of CeO_2-COS-50°C-3h. But the enhancement of sulfation time up to 24h increases the integral area of CeO_2-CS_2+COS-50°C-3h at region II, and CeO_2-CS_2+COS-50°C-24h presents the highest reduction temperature of SO_4^{2-} species. In addition, the integrated areas of the reduction peak in the III region of the sulfated catalysts are larger than that of CeO_2. These all indicate that the gas-phase sulfation of organic CS_2 or/and COS at 50 °C contributes to enhancing the mobility of lattice oxygen of cubic fluorite CeO_2 [85], and CeO_2-CS_2-50°C-3h presents the best mobility of lattice oxygen and the largest

527 concentration of adsorbed oxygen, which is in accordance with the results of Raman and XPS

528 spectra.

529 **Table 5.** The calculated peak areas for the H_2-TPR spectra of catalysts.

Samples	H_2-TPR peak area (a.u.)		
	I	II	III
CeO_2	922	-	1274
CeO_2-CS_2-50°C-3h	729	5282	1929
CeO_2-COS-50°C-3h	479	7065	1887
CeO_2-CS_2+COS-50°C-3h	462	6550	1956
CeO_2-CS_2+COS-50°C-24h	369	6977	2012

530

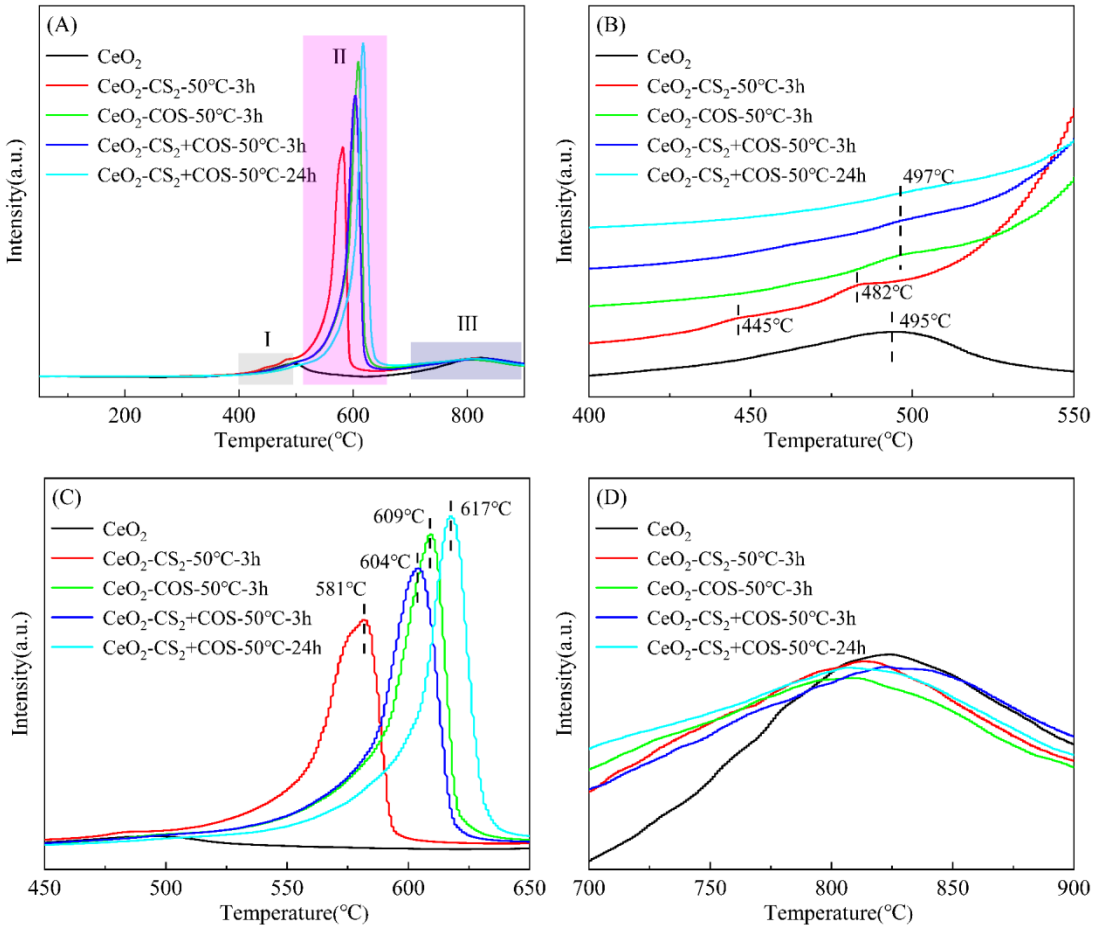

531

532 **Fig. 11.** The H_2-TPR profiles of CeO_2, CeO_2-CS_2-50°C-3h, CeO_2-COS-50°C-3h, CeO_2-CS_2+COS-50°C-3h and

CeO_2-CS_2+COS-50°C-24h catalysts.

3.2.7. The properties of surface acidity

The surface acidity is widely recognized as a pivotal factor on influencing the catalytic reactions. In order to investigate the acid characteristics and quantity of the as-prepared catalysts, Fourier transform infrared (Py-IR) measurements of pyridine desorption were conducted at 150 °C and 300 °C, which are associated with weak acid sites and medium-strong acid sites, respectively [86]. As illustrated in Figure 12, the band at 1540 cm^{-1} corresponds to pyridine adsorption on the Brønsted acid site [87], while bands at 1442 cm^{-1}, 1575 cm^{-1}, and 1600 cm^{-1} signify pyridine adsorption on the Lewis acid site [88]. Furthermore, the band at 1489 cm^{-1} indicates the interaction of pyridine molecules with both Brønsted and Lewis acid sites [89]. As shown in Table 6, the quantity of Lewis acid sites and Brønsted acid sites was determined according to the Py-IR curves at 150 °C and 300 °C. Interestingly, CeO_2-CS_2-50°C-3h exhibits stronger surface acid sites, including both weak acid and medium-strong acid sites, than CeO_2-COS-50°C-3h, although less sulfate (SO_4^{2-}) and total sulfur content (S) formed on its surface according to the results of TG-DTG and XPS. This demonstrates that the kind of organic sulfur during the gas-phase sulfation at 50 °C can regulate the formed types and quality of sulfur-containing species in the as-prepared CeO_2 catalyst, which play different role on the formation of acid sites for catalyst, and the gas-phase sulfation of CS_2 at 50 °C brings much less sulfur-containing species compared to COS, but better promotional effect on the formation of acid sites. Xie also pointed out that larger sulfates might be disadvantageous to the formation of acid sites for catalyst [90]. Furthermore, the partial substitution of COS by CS_2 during the gas-phase sulfation improves both weak acid and medium-strong acid sites of CeO_2-COS-50°C-3h, and this promotional effect is further enhanced by extending the

555 sulfonation time to 24 h. And CeO_2-CS_2+COS-50ºC-24h presents stronger weak acid and medium-
556 strong acid sites than CeO_2-CS_2-50ºC-3h, although its low-temperature NO_x conversions are still
557 lower than the latter. It is worth noting that the B/L values in CeO_2-COS-50ºC-3h and CeO_2-
558 CS_2+COS-50ºC-24h catalysts are larger, which is usually thought to be related to more sulfate
559 species formed on the catalyst surfaces. Therefore, it can be inferred that the deposition of larger
560 sulfur-containing species, including sulfates and elemental sulfur, on the surface of CeO_2-
561 CS_2+COS-50ºC-24h catalyst might block the active sites, leading to less NH_3-SCR activity
562 compared to CeO_2-CS_2-50ºC-3h [22,91].

563

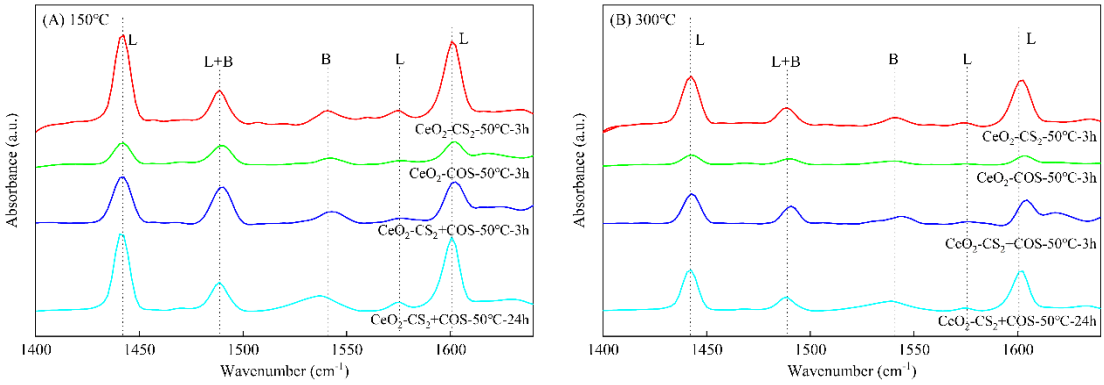

564 **Fig. 12.** The desorption spectra of pyridine for the as-prepared CeO_2-CS_2-50ºC-3h, CeO_2-COS-50ºC-3h, CeO_2-
565 CS_2+COS-50ºC-3h and CeO_2-CS_2+COS-50ºC-24h catalysts at (A) 150 ºC and (B) 300 ºC.

566 **Table 6.** The concentration and distribution of Lewis (L) and Brønsted (B) acid sites on the as-prepared CeO_2-CS_2-
567 50ºC-3h, CeO_2-COS-50ºC-3h, CeO_2-CS_2+COS-50ºC-3h and CeO_2-CS_2+COS-50ºC-24h catalysts.

Samples	Weak acid (μmol/g)				Medium-strong acid (μmol/g)			
	B	L	B/L	Total acid amount	B	L	B/L	Total acid amount
CeO_2-CS_2-50ºC-3h	25.66	99.68	0.257	125.34	16.37	58.15	0.282	74.52
CeO_2-COS-50ºC-3h	16.34	25.62	0.638	41.96	10.34	11.59	0.892	21.93
CeO_2-CS_2+COS-	29.89	60.92	0.491	90.81	19.65	35.25	0.609	54.90

$50^{o}C$-3h								
CeO_2-CS_2+COS-$50^{o}C$-24h	56.26	94.68	0.594	150.94	39.30	47.68	0.824	86.98

3.3 Discussion and long-time durability testing coupling re-cycle experiments

The results of TG, H_2-TPR and XPS show the influence of organic sulfur types on the formed amount of sulfate species (SO_4^{2-}) during the gas-phase sulfation of organic COS or/and CS_2 at 50 ^{o}C, which has been regarded as an important factor on the promotional effect of acid sites and NH_3-SCR activity of CeO_2 catalyst. Therefore, in order to investigate the relationship between the formed amount of sulfate species and the NH_3-SCR activity, the amount of sulfate species obtained through different characterization techniques were normalized based on CeO_2-CS_2-$50^{o}C$-3h. From Fig. 13, it can be found that the law of the calculated normalized sulfate content of TG, H_2-TPR and XPS are consistent, and the gas-phase sulfation of COS presents stronger promotional effect on the formation of sulfate than that of CS_2, although CeO_2-CS_2-$50^{o}C$-3h exhibits larger acid sites and the best NH_3-SCR activity. This indicates that the formed amount of sulfate might not be the determining factor on the NH_3-SCR activity of the sulfated CeO_2 catalysts by organic COS or/and CS_2 at 50 ^{o}C. Furthermore, the formed sulfate under the gas-phase sulfation of CS_2 might be more active based on the acid sites and the NH_3-SCR activity than those of COS, and the adsorption and transformation of COS and CS_2 are different on cubic fluorite CeO_2 surface at 50 ^{o}C. It should be mentioned that the formed amount of sulfate for COS+CS_2 falls between those of CS_2 or COS when the sulfation time is 3 h, and the enhancement of sulfation time up to 24 h increases the formed amount of sulfate slightly, but the value remains approximately the same as that of CeO_2-COS-$50^{o}C$-3h. This suggests that the adsorption of sulfate reaches a saturation point on cubic fluorite CeO_2 surface during the sulfation process of organic COS or/and CS_2 [27].

588 Based on the above characterization analysis, under the hydrolysis temperature of 50 °C, the

589 adsorption and conversion of CS_2 or/and COS over cubic fluorite CeO_2 are inferred as follows:

590 $$CS_2 + [O] \rightarrow COS + S \quad (6)$$

591 $$COS + [O] \rightarrow CO_2 \uparrow + S + SO_4^{2-} \quad (7)$$

592 $$S + [O] \rightarrow SO_2 \uparrow + SO_4^{2-} \quad (8)$$

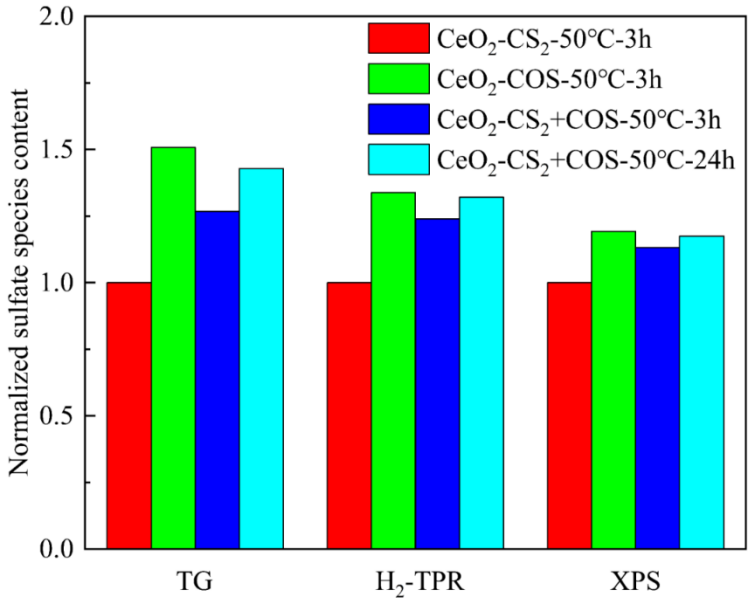

593

594 **Fig. 13.** Normalized sulfate content of different characterization techniques.

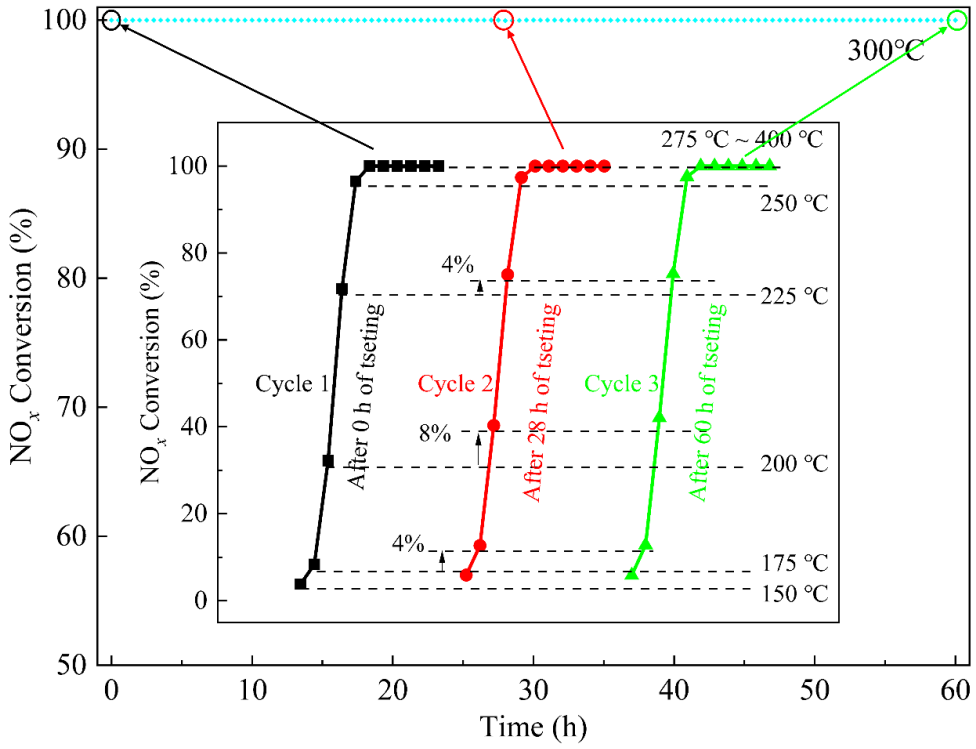

595

596 **Fig. 14.** The long-time durability testing at 300 ºC and re-cycle experiments of CeO_2-CS_2+COS-50ºC-24h catalyst.

597 Firstly, CS_2 could be adsorbed over CeO_2 and reacts with its surface inherent oxygen-
598 containing functional groups to generate S and COS. And then, the formed COS is adsorbed again
599 and oxidized to gas-phase CO_2, S and SO_4^{2-}, which are deposited or adsorbed on CeO_2 surfaces. In
600 the meantime, the deposited partial S can be further oxidized to SO_2 or/and SO_4^{2-} by the oxygen-
601 containing functional groups on the catalyst surfaces. Therefore, compared to COS, the reductive
602 CS_2 presents a stronger promotional effect on the formation of adsorbed oxygen and the mobility of
603 lattice oxygen on cubic fluorite CeO_2 surface, thus more deposited S can be oxidized to gas-phase
604 SO_2 for the gas-phase sulfation of CS_2 at 50 ºC than that of COS. As a result, CeO_2-CS_2-50°C-3h
605 exhibits less both sulfur and sulfate than CeO_2-COS-50ºC-3h. This also can explain the reduced
606 formation of sulfur and sulfate on CeO_2-CS_2+COS-50ºC-3h surface comparing to CeO_2-COS-50ºC-
607 3h. Furthermore, for the co-existence of COS+CS_2, the formed amount of sulfate does not increase
608 with the enhancement of sulfation time up to 24 h linearly, which might be attributed to the

609 consumption of the oxygen-containing functional groups on CeO_2 surfaces. Thus, more sulfur
610 deposits on the CeO_2-CS_2+COS-50°C-24h surface when the sulfation time increases from 3 h to 24
611 h. However, the depositing sulfur is easy to be oxidized to sulfur oxide or/and sulfates according to
612 the weight loss at 200~500 °C of TG-DTG (Fig. 9) and TG-MS (Fig. 10) for the sulfated CeO_2-
613 CS_2+COS-50°C-24h catalyst, which might affect its NH_3-SCR activity. Therefore, in order to
614 investigate the thermal stability of the sulfated CeO_2 catalyst by organic sulfur, the sulfated CeO_2-
615 CS_2+COS-50°C-24h catalyst had been re-calcined in air atmosphere at 400 °C for 5 h, and the
616 corresponding NH_3-SCR activity of CeO_2-CS_2+COS-50°C-24h-SC was given in Fig. S6 for
617 comparisons. As shown in Fig. S6, the re-calcination in air atmosphere at 400 °C only results in a
618 slight decrease in the NH_3-SCR activity of 200~300 °C for the sulfated CeO_2-CS_2+COS-50°C-24h
619 catalyst, and CeO_2-CS_2+COS-50°C-24h-SC also exhibits excellent catalytic performance of NO_x
620 reduction, demonstrating that the sulfated CeO_2 catalyst by organic sulfur at a hydrolysis
621 temperature presents a good stability for NH_3-SCR reaction. Furthermore, a long-time durability
622 testing at 300 °C coupling re-cycle experiments were also carried out for the sulfated CeO_2-
623 CS_2+COS-50°C-24h catalyst to study the stability of NH_3-SCR reaction. In addition, FTIR, Raman
624 and XPS were used to investigate the change of sulphate structure on the surface of CeO_2-CS_2+COS-
625 50°C-24h catalyst after the long-time durability testing at 300 °C coupling re-cycle experiments, and
626 the results are shown in Fig. 14, Fig 15 and Fig. S7, respectively.

627 As shown in Fig. 14, the sulfated CeO_2-CS_2+COS-50°C-24h catalyst presents a good stability
628 for NH_3-SCR reaction, and its NO_x conversion at 300 °C under the GHSV of 200,000 mL/(g·h)
629 keeps at 100% for up to 60 hours of testing. Interestingly, the results of the first re-cycle testing
630 demonstrate that the long-time testing at 300 °C for 28 h improves the low-temperature NH_3-SCR

631 activity of the sulfated CeO_2-CS_2+COS-50°C-24h catalyst, and the NO_x conversions at 175 °C,
632 200 °C and 225 °C during the first re-cycle testing increase by 4%, 8% and 4%, respectively.
633 Furthermore, this promoting effect is further enhanced by the following long-time testing of other
634 32 h. This demonstrates that the long-time durability testing coupling re-cycle experiments indeed
635 affects the NH_3-SCR activity of the sulfated CeO_2-CS_2+COS-50°C-24h catalyst via influencing the
636 conversion of the formed sulfur-containing species on the catalyst surfaces. The FTIR spectra
637 depicted in Fig. 15(A) indicates that there exist the bending and stretching vibrations of -OH group
638 (3415 cm^{-1} and 1628 cm^{-1}), the S-O and S=O bonds attributed to surface sulfates (1040 cm^{-1} and
639 979 cm^{-1}, inorganic chelating bidentate sulfates) and bulk sulfates (1120 cm^{-1}) for both CeO_2-
640 CS_2+COS-50°C-24h and CeO_2-CS_2+COS-50°C-24h-CT catalysts, respectively [92-94]. However,
641 CeO_2-CS_2+COS-50°C-24h-CT presents slightly weaker intensity of these FTIR peaks than CeO_2-
642 CS_2+COS-50°C-24h. This demonstrates that the long-time durability testing coupling re-cycle
643 experiments decreases the adsorbed capacity of sulfur-containing species on the surface of CeO_2-
644 CS_2+COS-50°C-24h catalyst. Interestingly, according to the results in Fig. 15(B), the long-time
645 durability testing coupling re-cycle experiments induces the appearance of a Raman peak at 998 cm^{-1},
646 which is attributed to the S-O asymmetric vibration of sulfate ions [25]. Meanwhile, this treatment
647 enhances the intensity of vibration band at 600 cm^{-1}, indicating the long-time durability testing
648 coupling re-cycle experiments contributes to improving the oxygen vacancy defects of the sulfated
649 CeO_2-CS_2+COS-50°C-24h catalyst effectively (Fig. S5). Furthermore, the results of XPS spectra in
650 Fig. S7, Fig. 15(C), Fig. 15(D) and Table 3 demonstrate that the long-time durability testing
651 coupling re-cycle experiments makes the binding energy attributed to the lattice oxygen (O_α) shift
652 to right and induces the disappearance of S 2p peak ascribed to sulfur element for the sulfated CeO_2-

CS_2+COS-50°C-24h catalyst. This indicates that the formed sulfur element of the sulfated CeO_2-CS_2+COS-50°C-24h catalyst could be slowly oxidized to sulfur oxides or/and sulfates during the long-time durability testing coupling re-cycle experiments. At the same time, both the concentration of Ce element and $O_\beta/(O_\alpha+O_\beta+O_\gamma)$ molar ratio on the catalyst surface are also improved. To sum up, the long-time durability testing coupling re-cycle experiments can lead to the oxidization of sulfur element to sulfur oxides or/and sulfates, optimizing the oxygen vacancy defects and increasing the concentration of chemisorbed oxygen of the sulfated CeO_2-CS_2+COS-50°C-24h catalyst. These phenomena indicate that the adsorption and conversion of sulfur-containing species on cubic fluorite CeO_2 surfaces might play an important role on the physical-chemical properties and the NH_3-SCR activity of the sulfated CeO_2 catalyst by organic CS_2 or/and COS.

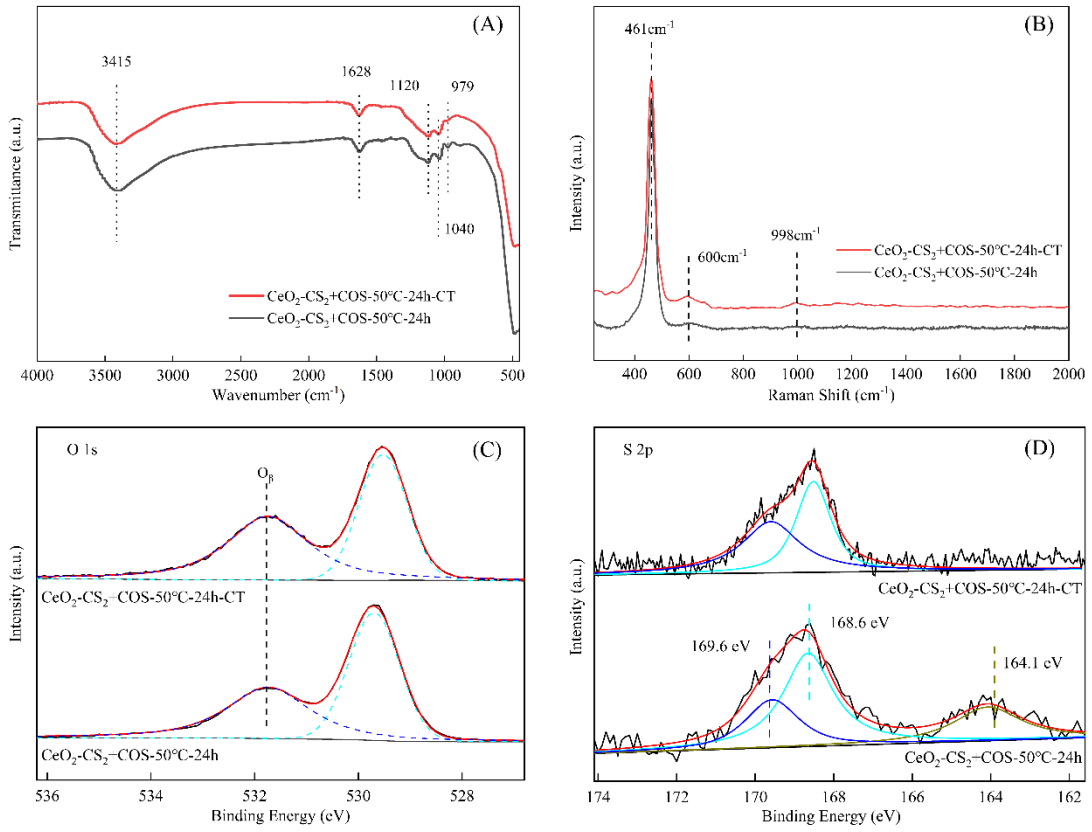

Fig. 15. The FTIR spectra (A), Raman Spectra (B) and XPS spectra of (C) O 1s and (D) S 2p for the CeO_2-CS_2+COS-50°C-24h and CeO_2-CS_2+COS-50°C-24h-CT catalysts.

3.4. Competitive adsorption analysis

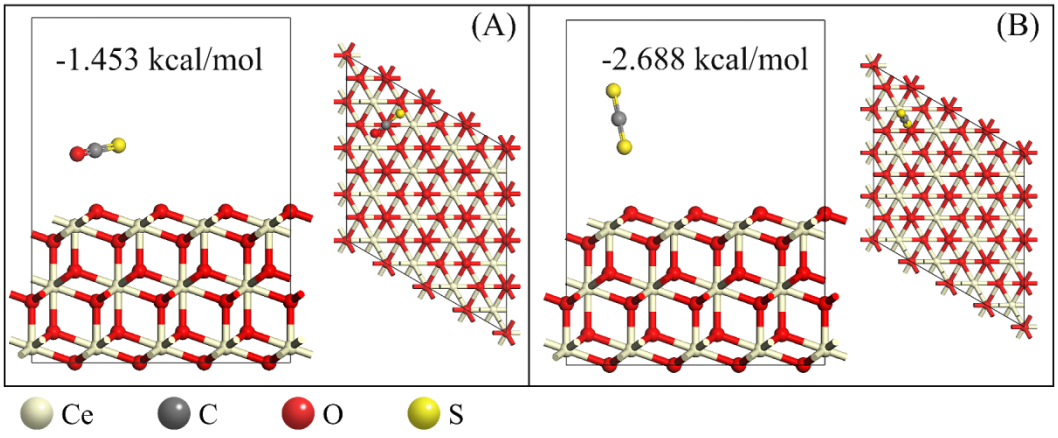

Fig. 16. The optimized geometry and calculated adsorption energy of COS and CS_2 on CeO_2 (111): (A) correspond to the adsorption of COS at O top site; (B) correspond to the adsorption of CS_2 at Ce-O bridge site.

In this study, the adsorption energy of COS and CS_2 on the optimized CeO_2 (111) crystal plane were calculated to reveal their competitive adsorption on the catalyst surface. As shown in Fig. S8 and Fig. 16, four adsorption configurations of COS/CS_2 on CeO_2 (111) were involved: O-top site, Ce-top site, O-O bridge site, and Ce-O bridge site. The results indicate that the most stable adsorption configuration of COS involved the bonding of the S atom in COS to the O-top atom of CeO_2 (111) crystal plane (Fig. 16(A)), with an absolute adsorption energy value in the order of O-top site (1.453 eV) > Ce-O bridge site (1.316 eV) > Ce-top site (0.517 eV) > O-O bridge site (0.451 eV). Similarly, for CS_2, the absolute value of the adsorption energy is in the order of Ce-O bridge site (2.688 eV) > O-O bridge site (2.600 eV) > Ce-top site (2.480 eV) > O-top site (2.158 eV), indicating that the most stable adsorption configuration of CS_2 is the bonding of the S atom in CS_2 to the Ce-O bridge site of CeO_2 (111) crystal plane (Fig. 16(B)). The calculated adsorption energy of CS_2 on the CeO_2 (111) crystal plane is stronger than that of COS. The adsorption energy of gas molecules on the material surface is determined by their electronic structure and the molecules with unsaturated chemical bonds have a stronger adsorption capacity due to their stronger chemical bonds

with surface atoms [95-97]. Basically, the hydrolysis process of organic sulfur involves three steps: adsorption, activation and hydrolysis. Hence, higher adsorption energy is beneficial for the adsorption of organic sulfur gas on the catalysts surface, which in turn is favorable for the subsequent reaction process [39,98]. However, it is worth noting that although the adsorption energy of CS_2 on CeO_2 (111) crystal plane is higher than that of COS, more sulfate species (TG, XPS, H_2-TPR) are generated in CeO_2 during the sulfation of COS. Sui et al. [99] found that the 1% Cu^{2+}/Al_2O_3 catalyst with the lowest adsorption capacity of CS_2, presented the excellent conversion of CS_2 and had larger formation of sulfate/sulfite species on its surface, which indicated that there was no correlation between the adsorption capacity and conversion of CS_2. Based on the calculated adsorption energy and the formed amount of sulfate species, it is clear that there is no intrinsic relationship between the adsorption capacity of COS/CS_2 on CeO_2 surface and the formed amount of sulfate species.

4. Conclusions

In this study, the gas-phase sulfation of CS_2 or/and COS was carried out at the hydrolysis temperature of organic sulfur for the first time to improve the NH_3-SCR activity of CeO_2 catalyst. Compared with the previous sulfation treatment of CeO_2 with CS_2/COS at 300 °C, the gas-phase sulfation at 50 °C exhibits a more prominent promotion effect on the NH_3-SCR activity. The results show that CeO_2-CS_2-50°C-3h exhibits the best NO_x reduction performance, while there exists a competitive adsorption relationship between CS_2 and COS when they coexist in sulfurized flue gas, which could negate this promoting effect. The characterization results show that the adsorption and conversion of sulfur-containing species on cubic fluorite CeO_2 surfaces play an important role on the physical-chemical properties and the NH_3-SCR activity of the sulfated CeO_2 catalyst by organic

706 CS_2 or/and COS. The gas-phase sulfation of organic CS_2 or/and COS at 50 °C contributes to
707 enhancing the mobility of lattice oxygen of cubic fluorite CeO_2 and the concentration of oxygen
708 defects for the sulfated CeO_2 catalyst, but the adsorption and transformation of COS and CS_2 are
709 different on cubic fluorite CeO_2 surface at 50 °C, and the kinds of organic COS/CS_2 can regulate the
710 formed types and quality of sulfur-containing species on the catalyst surfaces during the gas-phase
711 sulfation at 50 °C. In addition, the formed sulfates under the gas-phase sulfation of CS_2 might be
712 more active than those of COS, although the gas-phase sulfation of COS presents stronger
713 promotional effect on the formation of sulfates than that of CS_2. Furthermore, the competitive
714 adsorption and conversion of CS_2 and COS is disadvantageous for the formation of oxygen
715 vacancies on the catalyst surfaces compared to single CS_2 or COS. However, the long-time
716 durability testing coupling re-cycle experiments leads to the oxidization of sulfur element to sulfur
717 oxides or/and sulfates, optimizing the oxygen vacancy defects and increasing the concentration of
718 chemisorbed oxygen of the sulfated CeO_2-CS_2+COS-50°C-24h catalyst, thereby improves its NH_3-
719 SCR activity. And the sulfated CeO_2 catalyst by the gas-phase sulfation of organic COS+CS_2
720 presents a good stability for NH_3-SCR reaction. This study specifies a novel approach to simplify
721 the gas-phase sulfation process of CeO_2 catalyst, which is valuable in promotion of the NH_3-SCR
722 activity of CeO_2 and reduction of cost in experimental procedures.

723 # CRediT authorship contribution statement

724 **Zhibo Xiong:** Conceptualization, Funding acquisition, Writing - review & editing. **Zhenchang Sun and**
725 **Jiaxing Liu:** Writing - original draft, Methodology, Validation. **Yanping Du:** Methodology, Writing - review &
726 editing. **Yafei Zhu:** Software, Methodology. **Fei Zhou:** Investigation, Supervision. **Jing Jin:** Investigation,
727 Supervision, Writing - review & editing, Funding acquisition. **Qiguo Yang:** Investigation, Supervision, Writing -

review & editing. **Wei Lu:** Investigation, Supervision, Funding acquisition.

Declaration of Competing Interest

The authors declare that they have no known competing financial interests or personal relationships that could have appeared to influence the work reported in this paper.

Acknowledgements

This work was supported by the National Science Foundation of China (No. 51406118), the Bureau of Shanghai Municipal Science and Technology (No. 23010503500), Program of Special Appointment (Eastern Scholar) at Shanghai Institutions of Higher Learning (No. QD2015017).

References

[1] Z. Sun, J.P. Liu, Z.Q. Sun, Synergistic decarbonization and desulfurization of blast furnace gas via a novel magnesium-molybdenum looping process, Fuel 279 (2020) 118418, https://doi.org/10.1016/j.fuel.2020.118418.

[2] X. Song, K. Lia, C. Wang, X. Sun, P. Ning, L.H. Tang, Regeneration performance and mechanism of modified walnut shell biochar catalyst for low temperature catalytic hydrolysis of organic sulfur, Chem. Eng. J. 330 (2017) 727-735, http://dx.doi.org/10.1016/j.cej.2017.08.016.

[3] J. Kima, J.Y. Do, K. Nahm, No. Park, J. Chi, J.P. Hong, M. Kang, Capturing ability for COS gas by a strong bridge bonding of a pair of potassium anchored on carbonate of activated carbon at low temperatures, Sep. Purif. Technol. 211 (2019) 421-429, https://doi.org/10.1016/j.seppur.2018.10.013.

[4] N. Liu, P. Ning, X. Sun, C. Wang, X. Song, F. Wang, K. Li, Simultaneous catalytic hydrolysis of HCN, COS and CS_2 over metal-modified microwave coal-based activated carbon, Sep. Purif. Technol. 259 (2021) 118205, https://doi.org/10.1016/j.seppur.2020.118205.

[5] P.T. Gao, Y.R. Li, Y.T. Lin, L.P. Chang, T.Y. Zhu, Promoting effect of Fe/La loading on γ-Al_2O_3 catalyst for

hydrolysis of carbonyl sulfur, Environ. Sci. Pollut. R. 29 (2022) 84166-84179, https://doi.org/10.1007/s11356-022-20928-1.

[6] K.K. Pandey, Reactivities of carbonyl sulfide (COS), carbon disulfide (CS_2) and carbon dioxide (CO_2) with transition metal complexes, Coordin. Chem. Rev. 140 (1995) 37-114, https://doi.org/10.1016/0010-8545(94)01120-Z.

[7] X. Song, K. Li, P. Ning, C. Wang, X. Sun, L.H. Tang, H.T. Ruan, S. Han, Surface characterization studies of walnut-shell biochar catalysts for simultaneously removing of organic sulfur from yellow phosphorus tail gas, Appl. Surf. Sci. 42 (2017) 130-140, https://doi.org/10.1016/j.apsusc.2017.06.328.

[8] L. Wang, M.Y. Liu, S. Ren, X.D. Li, Z.C. Chen, M.M. Wang, T. Chen, J. Yang, Recent advance for NO_x removal with carbonaceous material for low-temperature NH_3-SCR reaction, Catalysis Today 418 (2023) 114053, https://doi.org/10.1016/j.cattod.2023.114053.

[9] S.J. Hu, J.N. Gu, K. Li, J.X. Liang, Y.X. Xue, X. Min, M.M. Guo, X.F. Hu, J.P. Jia, T.H. Sun, Boosting COS catalytic hydrolysis performance over Zn-Al oxide derived from ZnAl hydrotalcite-like compound modified via the dopant of rare earth metals and the replacement of precipitation base, Appl. Surf. Sci. 599 (2022) 154016, https://doi.org/10.1016/j.apsusc.2022.154016.

[10] H.K. Jin, Z.Y. An, Q.C. Li, Y.Q. Duan, Z.H. Zhou, Z.K. Sun, L.B. Duan, Catalysts of Ordered Mesoporous Alumina with a Large Pore Size for Low-Temperature Hydrolysis of Carbonyl Sulfide, Energy & Fuels 35 (2021) 8895-8908, https://doi.org/10.1021/acs.energyfuels.1c00475.

[11] J.X. Qu, X.Q. Wang, L.L. Wang, B.W. Xu, P. Ning, Y.X. Ma, Y.B. Xie, R. Cao, Q. Ma, The investigation of the role of nitrogen in the improvement of catalytic activity and stability of Zr/Ti-based material for carbon disulfide hydrolysis, Sep. Purif. Technol. 296 (2022) 121357, https://doi.org/10.1016/j.seppur.2022.121357.

[12] R. Cao, P. Ning, X.Q. Wang, L.L. Wang, Y.X. Ma, Y.B. Xie, H. Zhang, J.X. Qu, Low-temperature hydrolysis

of carbonyl sulfide in blast furnace gas using Al_2O_3-based catalysts with high oxidation resistance, Fuel 310 (2022) 122295, https://doi.org/10.1016/j.fuel.2021.122295.

[13] H.Y. Wang, H.H. Yi, X.L. Tang, P. Ning, L.L. Yu, D. He, S.Z. Zhao, K. Li, Catalytic hydrolysis of COS over calcined CoNiAl hydrotalcite-like compounds modified by cerium, Appl. Clay. Sci. 70 (2012) 8-13, http://dx.doi.org/10.1016/j.clay.2012.09.008.

[14] Y.Q. Zhang, Z.B. Xiao, J.X. Ma, Hydrolysis of carbonyl sulfide over rare earth oxysulfides, Appl. Catal. B: Environ 48 (2004) 57-63, https://doi.org/10.1016/j.apcatb.2003.09.015.

[15] P. Wu, Y.P. Zhang, Y.L. Liu, H.Q. Yang, K. Shen, G.B. Li, S. Wang, S.P. Ding, S.L. Zhang, Experimental and theoretical research on pore-modified and K-doped Al_2O_3 catalysts for COS hydrolysis: The role of oxygen vacancies and basicity, Chem. Eng. J. 450 (2022) 138091, https://doi.org/10.1016/j.cej.2022.138091.

[16] Y.L. Liu, P. Wu, K. Shen, Y.P. Zhang, G.B. Li, B. Li, Contribution of Na/K Doping to the Activity and Mechanism of Low-Temperature COS Hydrolysis over TiO_2-Al_2O_3 Based Catalyst in Blast Furnace Gas, ACS Omega 7 (2022) 13299-13312, https://doi.org/10.1021/acsomega.2c00968.

[17] Z. Wei, X. Zhang, F.L. Zhang, Q. Xie, S.Z. Zhao, Z.P. Hao, Boosting carbonyl sulfide catalytic hydrolysis performance over N-doped Mg-Al oxide derived from MgAl-layered double hydroxide, J. Hazard. Mater. 407 (2021) 124546, https://doi.org/10.1016/j.jhazmat.2020.124546.

[18] Z.B. Xiong, Z.Z. Li, C.X. Li, W. Wang, W. Lu, Y.P. Du, S.L. Tian, Green synthesis of Tungsten-doped CeO_2 catalyst for selective catalytic reduction of NO_x with NH_3 using starch bio-template, Appl. Surf. Sci. 536 (2021) 147719, https://doi.org/10.1016/j.apsusc.2020.147719.

[19] Z.X. Song, Y. Xing, X.J. Zhang, H. Zhao, M. Zhao, J.G. Zhao, Z.A. Ma, Q.L. Zhang, Silicotungstic acid modified Ce-Fe-O_x catalyst for selective catalytic reduction of NO_x with NH_3: Effect of the amount of HSiW, Appl. Organomet. Chem. 33 (2019) e5160, https://doi.org/10.1002/aoc.5160.

794 [20] Z.X. Song, L.Y. Wang, Q.L. Zhang, P. Ning, J. Hu, T. Tang, X. Liu, B. Li, Mechanisms study of silicotungstic
795 acid modified CeO_2 catalyst for selective catalytic reduction of NO_x with NH_3: Effect of pH values, J Taiwan.
796 Inst. Chem. E. 91 (2018) 243-250, https://doi.org/10.1016/j.jtice.2018.05.018.
797 [21] Z.X. Song, P. Ning, Q.L. Zhang, X. Liu, J.H. Zhang, Y.C. Wang, Y.K. Duan, Z.Z. Huang, The role of surface
798 properties of silicotungstic acid doped CeO_2 for selective catalytic reduction of NO_x by NH_3: Effect of
799 precipitant, J. Mol. Catal. A-Chem. 413 (2016) 15-23, http://dx.doi.org/10.1016/j.molcata.2015.12.009.
800 [22] W.J. Zhang, G.F. Liu, J. Jiang, Y.C. Tan, Q. Wang, C.H. Gong, D.K. Shen, C.F. Wu, Sulfation effect of Ce/TiO_2
801 catalyst for the selective catalytic reduction of NO_x with NH_3: mechanism and kinetic studies, RSC Adv. 9
802 (2019) 32110, https://doi.org/10.1039/C9RA06985B.
803 [23] D.W. Kwon, J. Kim, H.P. Ha, Establishment of surface/bulk-like species functionalization by controlling the
804 sulfation temperature of Sb/V/Ce/Ti for NH_3-SCR, Appl. Surf. Sci. 481 (2019) 1503-1514,
805 https://doi.org/10.1016/j.apsusc.2019.03.218.
806 [24] Q. Wu, X.P. Chen, J.X. Mi, S.X. Cai, L. Ma, W.T. Zhao, J.J. Chen, J.H. Li, The Absence of Oxygen in Sulfation
807 Promotes the Performance of the Sulfated CeO_2 Catalyst for Low-Temperature Selective Catalytic Reduction
808 of NO_x by NH_3: Redox Property versus Acidity, ACS. Sustain. Chem. Eng. 9 (2021) 967-979,
809 https://dx.doi.org/10.1021/acssuschemeng.0c08427.
810 [25] W. Tan, J.M. Wang, S.H. Yu, A.N. Liu, L.L. Li, K. Guo, Y.D. Luo, S.H. Xie, F. Gao, F.D. Liu, L. Dong,
811 Morphology-Sensitive Sulfation Effect on Ceria Catalysts for NH_3-SCR, Top. Catal. 63 (2020) 932-943,
812 https://doi.org/10.1007/s11244-020-01342-8.
813 [26] S.H. Wang, C. Fan, Z.Q. Zhao, Q. Liu, G. Xu, M.H. Wu, J.J. Chen, J.H. Li, A facile and controllable in situ
814 sulfation strategy for CuCeZr catalyst for NH_3-SCR, Appl. Catal. A: General 597 (2020) 117554,
815 https://doi.org/10.1016/j.apcata.2020.117554.

816 [27] Q. Xie, Y.D. Cai, L. Zhang, Z.H. Hu, T.Z. Li, X.D. Wang, Q. Zeng, X. Wang, J.F. Sun, L. Dong, Relationships
817 between Adsorption Amount of Surface Sulfate and NH_3-SCR Performance over CeO_2, J. Phys. Chem. C 125
818 (2021) 21964-21974, https://doi.org/10.1021/acs.jpcc.1c06384.
819 [28] L. Zhang, W.X. Zou, K.L. Ma, Y. Cao, Y. Xiong, S.G. Wu, C.J. Tang, F. Gao, L. Dong, Sulfated Temperature
820 Effects on the Catalytic Activity of CeO_2 in NH_3-Selective Catalytic Reduction Conditions, J. Phys. Chem. C
821 119 (2015) 1155-1163, https://doi.org/10.1021/jp511282c.
822 [29] W. Wang, Z.B. Xiong, J. Jin, W. Lu, H.C. Shi, Influence of CS_2 pretreatment on the NH_3-SCR activity of CeO_2:
823 Synergistic promotional effect of sulfation and reduction, J. Environ. Chem. Eng. 9 (2021) 106836,
824 https://doi.org/10.1016/j.jece.2021.106836.
825 [30] X. Sun, P. Ning, X.L. Tang, H.H. Yi, K. Li, D. He, X.M. Xu, B. Huang, R.Y. Lai, Simultaneous catalytic
826 hydrolysis of carbonyl sulfide and carbon disulfide over Al_2O_3-K/CAC catalyst at low temperature, J. Energy.
827 Chem. 23 (2014) 221-226, https://doi.org/10.1016/S2095-4956(14)60139-X.
828 [31] X. Sun, H.T. Ruan, X. Song, L.N. Sun, K. Li, P. Ning, C. Wang, Research into the reaction process and the
829 effect of reaction conditions on the simultaneous removal of H_2S, COS and CS_2 at low temperature, RSC Adv.
830 8 (2018) 6996, https://doi.org/10.1039/c7ra12086a.
831 [32] W.Q. Xu, H. He, Y.B. Yu, Deactivation of a Ce/TiO_2 Catalyst by SO_2 in the Selective Catalytic Reduction of
832 NO by NH_3, J. Phys. Chem. C 113 (2009) 4426-4432, https://doi.org/10.1021/jp8088148.
833 [33] Y. Shi, S. Tan, X.X. Wang, M.F. Li, S.J. Li, W. Li, Regeneration of sulfur-poisoned CeO_2 catalyst for NH_3-
834 SCR of NO_x, Catal. Commun. 86 (2016) 67-71, http://dx.doi.org/10.1016/j.catcom.2016.08.004.
835 [34] Z.Z. Zhou, J.M. Lan, L.Y. Liu, Z.M. Liu, Enhanced alkali resistance of sulfated CeO_2 catalyst for the reduction
836 of NO_x from biomass fired flue gas, Catal. Commun. 149 (2021) 106230,
837 https://doi.org/10.1016/j.catcom.2020.106230.

[35] W. Wang, Z.B. Xiong, W.F. He, W. Lu, H.C. Shi, Influence of thiourea modification on the NH_3-SCR activity of CeO_2: Simultaneous tuning morphology and surface acidity, J. Energy Inst 98 (2021) 322-333, https://doi.org/10.1016/j.joei.2021.07.009.

[36] X. Li, X.Q. Wang, L.L. Wang, P. Ning, Y.X. Ma, L. Zhong, Y. Wu, L. Yuan, Efficient removal of carbonyl sulfur and hydrogen sulfide from blast furnace gas by one-step catalytic process with modified activated carbon, Appl. Surf. Sci. 579 (2022) 152189, https://doi.org/10.1016/j.apsusc.2021.152189.

[37] Y. Wang, G.J. Zhang, X. Shi, L.H. Tang, Z.Y. Ning, New insights in the hydrolysis mechanism of carbon disulfide (CS_2): a density functional study, Struct. Chem. 34 (2023) 71-82, https://doi.org/10.1007/s11224-022-01963-7.

[38] J.P. Perdew, K. Burke, M. Ernzerhof, Generalized Gradient Approximation Made Simple, Phys. Rev. Lett. 77 (1996) 3865-3868, https://doi.org/10.1103/PhysRevLett.77.3865.

[39] X. Li, X.Q. Wang, L.L. Wang, L. Yuan, Y.X. Ma, Y.B. Xie, Y.R. Xiong, P. Ning, Alkali-induced metal-based coconut shell biochar for efficient catalytic removal of H_2S at a medium–high temperature in blast furnace gas with significantly enhanced S selectivity, Sep. Purif. Technol. 306 (2023) 122698, https://doi.org/10.1016/j.seppur.2022.122698.

[40] X. Song, P. Ning, C. Wang, K. Li, L.H. Tang, X. Sun, Catalytic hydrolysis of COS over CeO_2 (110) surface: A density functional theory study, Appl. Surf. Sci. 414 (2017) 345-352, http://dx.doi.org/10.1016/j.apsusc.2017.04.119.

[41] S.Z. Zhao, H.H. Yi, X.L. Tang, P. Ning, H.Y. Wang, D. He, Effect of Ce-doping on catalysts derived from hydrotalcite-like precursors for COS hydrolysis, J. Rare Earths 28 (2010) 329, https://doi.org/10.1016/S1002-0721(10)60341-9.

[42] S. Han, H. Yang, P. Ning, K. Li, L.H. Tang, C. Wang, X. Sun, X. Song, Density functional theory study on the

hydrolysis process of COS and CS_2 on a graphene surface, Res. Chem. Intermediat. 44 (2018) 2637-2651, https://doi.org/10.1007/s11164-018-3251-1.

[43] Y.F. Wang, L. Ding, H.M. Long, J.J. Xiao, L.X. Qian, H.T. Wang, C.B. Xu, Carbonyl sulfur removal from blast furnace gas: Recent progress, application status and future development. Chemosphere 307 (2022) 136090, https://doi.org/10.1016/j.chemosphere.2022.136090.

[44] D. Chiche, J.M. Schweitzer, Investigation of competitive COS and HCN hydrolysis reactions upon an industrial catalyst: Langmuir-Hinshelwood kinetics modeling. Appl. Catal. B: Environ 205 (2017) 189-200, http://dx.doi.org/10.1016/j.apcatb.2016.12.002.

[45] W. Tan, J.M. Wang, L.L. Li, A.N. Liu, G. Song, K. Guo, Y.D. Luo, F.D. Liu, F. Gao, L. Dong, Gas phase sulfation of ceria-zirconia solid solutions for generating highly efficient and SO_2 resistant NH_3-SCR catalysts for NO removal, J. Hazard. Mater. 388 (2020) 121729, https://doi.org/10.1016/j.jhazmat.2019.121729.

[46] J.W. Ji, L. Han, W. Song, J.F. Sun, W.X. Zou, C.J. Tang, L. Dong, Promotion effect of bulk sulfates over CeO_2 for selective catalytic reduction of NO by NH_3 at high temperatures, Chinese. Chem. Lett. 34 (2023) 107769, https://doi.org/10.1016/j.cclet.2022.107769.

[47] H.P. Liu, S.C. Xiong, H.J. Ou, H.H. Lei, J.J. Li, L. He, J.H. Li, The Contradictory Impact of Sulfation on a CeO_x/TiO_2 NH_3-SCR Catalyst: A Combined Experimental and DFT Study, Energ. Fuel. 37 (2023) 6674-6682, https://doi.org/10.1021/acs.energyfuels.3c00689.

[48] J.W. Ji, M.Z. Jing, X.W. Wang, W. Tan, K. Guo, L.L. Li, X. Wang, W. Song, L.J. Cheng, J.F. Sun, W.Y. Song, C.J. Tang, J. Liu, L. Dong, Activating low-temperature NH_3-SCR catalyst by breaking the strong interface between acid and redox sites: A case of model $Ce_2(SO_4)_3$-CeO_2 study, J. Catal. 399 (2021) 212-223, https://doi.org/10.1016/j.jcat.2021.05.001.

[49] X.R. Qi, L.P. Han, J. Deng, T.W. Lan, F.L. Wang, L.Y. Shi, D.S. Zhang, SO_2-Tolerant Catalytic Reduction of

882 NO_x via Tailoring Electron Transfer between Surface Iron Sulfate and Subsurface Ceria, Environ. Sci. Technol.
883 56 (2022) 5840-5848, https://doi.org/10.1021/acs.est.2c00944.
884 [50] X.J. Yao, Z. Wang, S.H. Yu, F.M. Yang, L. Dong, Acid pretreatment effect on the physicochemical property
885 and catalytic performance of CeO_2 for NH_3-SCR, Appl. Catal. A: General 542 (2017) 282-288,
886 http://dx.doi.org/10.1016/j.apcata.2017.06.003.
887 [51] X.X. Wang, H.Y. Ma, B.L. Li, Y.Q. Wang, S.H. Zhang, W. Li, S.J. Li, A superior cerium-tungsten bimetal
888 oxide catalyst with flower-like structure for selective catalytic reduction of NO_x by NH_3, Chem. Eng. J. 435
889 (2022) 134892, https://doi.org/10.1016/j.cej.2022.134892.
890 [52] X. Fang, Y.J. Liu, L.Z. Chen, Y. Cheng, Influence of surface active groups on SO_2 resistance of birnessite for
891 low-temperature NH_3-SCR, Chem. Eng. J. 399 (2020) 125798, https://doi.org/10.1016/j.cej.2020.125798.
892 [53] R.Y. Xie, L. Ma, K. Sun, G. Zhou, Z. Qu, N.Q. Yan, Catalytic performance and mechanistic evaluation of
893 sulfated CeO_2 cubes for selective catalytic reduction of NO_x with ammonia, J. Hazard. Mater. 420 (2021)
894 126545, https://doi.org/10.1016/j.jhazmat.2021.126545.
895 [54] O.A. Shilova, A.M. Nikolaev, A.S. Kovalenko, A.A. Sinel'nikov, Kh.E. Yorov, N.V. Tsvigun, V.V. Volkov, T.V.
896 Khamova, G.G. Panova, G.P. Kopitsa, Aqueous chemical synthesis of iron oxides magnetic nanoparticles of
897 different morphology and mesostructured, Ceram. Int. 47 (2021) 28866-28873,
898 https://doi.org/10.1016/j.ceramint.2021.07.047.
899 [55] X.H. Zheng, J.M. Cai, Y.N. Cao, L.J. Shen, Y. Zheng, F.J. Liu, S.J. Liang, Y.H. Xiao, L.L. Jiang, Construction
900 of cross-linked δ-MnO_2 with ultrathin structure for the oxidation of H_2S: Structure-activity relationship and
901 kinetics study, Appl. Catal. B: Environ 297 (2021) 120402, https://doi.org/10.1016/j.apcatb.2021.120402.
902 [56] X.H. Zheng, Y.L. Li, L.Y. Zhang, L.J. Shen, Y.H. Xiao, Y.F. Zhang, C. Au, L.L. Jiang, Insight into the effect
903 of morphology on catalytic performance of porous CeO_2 nanocrystals for H_2S selective oxidation, Appl. Catal.

B: Environ 252 (2019) 98-110, https://doi.org/10.1016/j.apcatb.2019.04.014.

[57] F.G. Sun, J. Liu, H.C. Chen, Z.X. Zhang, W.M. Qiao, D.H. Long, L.C. Ling, Nitrogen-Rich Mesoporous Carbons: Highly Efficient, Regenerable Metal-Free Catalysts for Low-Temperature Oxidation of H_2S, ACS Catal. 3 (2013) 862-870, https://doi.org/10.1021/cs300791j.

[58] P. Zhang, A. Chen, T.W. Lan, X.Y. Liu, T.T. Yan, W. Ren, D.S. Zhang, Balancing acid and redox sites of phosphorylated CeO_2 catalysts for NO_x reduction: The promoting and inhibiting mechanism of phosphorus, J. Hazard. Mater. 441 (2023) 129867, https://doi.org/10.1016/j.jhazmat.2022.129867.

[59] S. Loridant. Raman spectroscopy as a powerful tool to characterize ceria-based catalysts, Catal. Today. 373 (2021) 98-111, https://doi.org/10.1016/j.cattod.2020.03.044.

[60] R. Verma, S.K. Samdarshi, S. Bojja, S. Paul, B. Choudhury, A novel thermophotocatalyst of mixed-phase cerium oxide (CeO_2/Ce_2O_3) homocomposite nanostructure: Role of interface and oxygen vacancies, Sol. Energ. Mat. Sol. C 141 (2015) 414-422, http://dx.doi.org/10.1016/j.solmat.2015.06.027.

[61] W.X. Zou, C.Y. Ge, M.Y. Lu, S.G. Wu, Y.Z. Wang, J.F. Sun, Y. Pu, C.J. Tang, F. Gao, L. Dong. Engineering the NiO/CeO_2 interface to enhance the catalytic performance for CO oxidation, RSC Adv. 5 (2015) 98335, https://doi.org/10.1039/C5RA20466F.

[62] X.J. Zhang, Y. Xing, Z.X. Song, H. Zhao, M. Zhao, J.G. Zhao, Z.A. Ma, P.P. Zhang, N. Tsubaki, Comparison of support synthesis methods for TiO_2 and the effects of surface sulfates on its activity toward NH_3-SCR, New J. Chem. 43 (2019) 1818-1826, https://doi.org/10.1039/c8nj04363a.

[63] Y.H. Zhou, S. Ren, J. Yang, W.Z. Liu, Z.H. Su, Z.C. Chen, M.M. Wang, L. Chen, Effect of oxygen vacancies on improving NO oxidation over CeO_2 {111} and {100} facets for fast SCR reaction, J. Environ. Chem. Eng. 9 (2021) 106218, https://doi.org/10.1016/j.jece.2021.106218.

[64] C. Zhang, J.C. Li, D.L. Fang, P. Tan, L. Ma, Q.Y. Fang, G. Chen, Research progress on anti-poisoning of Mn-

based low temperature SCR catalysts, Clean. Coal Technol. 28 (2022) 110-135, https://10.13226/j.issn.1006-6772.HK22072501.

[65] R.J. Chi, X.Q. Wang, Y. Liu, Z.B. Wu, Highly active alkali etching silica-modified Cu-Ce-Ti catalyst with superior water resistance for low temperature NO_x reduction, Appl. Surf. Sci. 627 (2023) 157304, https://doi.org/10.1016/j.apsusc.2023.157304.

[66] X.D. Li, S. Ren, Z.C. Chen, L. Chen, M.M. Wang, L. Wang, A.P. Wang, Promoting mechanism of CuO on catalytic performance of CeFe catalyst for simultaneous removal of NO_x and CO, Fuel 347 (2023) 128435, https://doi.org/10.1016/j.fuel.2023.128435.

[67] D.K. Chen, D.D. He, J.C. Lu, L.P. Zhong, F. Liu, J.P. Liu, J. Yu, G.P. Wan, S.F. He, Y.M. Luo, Investigation of the role of surface lattice oxygen and bulk lattice oxygen migration of cerium-based oxygen carriers: XPS and designed H_2-TPR characterization, Appl. Catal. B: Environ 218 (2017) 249-259, http://dx.doi.org/10.1016/j.apcatb.2017.06.053.

[68] Y. Li, S.X. Cai, P.L. Wang, T.T. Yan, J.P. Zhang, D.S. Zhang, Improved NO_x Reduction over Phosphate-Modified Fe_2O_3/TiO_2 Catalysts Via Tailoring Reaction Paths by In Situ Creating Alkali-Poisoning Sites, Environ. Sci. Technol. 55 (2021) 9276-9284, https://doi.org/10.1021/acs.est.1c01722.

[69] S. Gao, X.B. Chen, H.Q. Wang, J.S. Mo, Z.B. Wu, Y. Liu, X.L. Weng, Ceria supported on sulfated zirconia as a superacid catalyst for selective catalytic reduction of NO with NH_3, J. Colloid. Interf. Sci. 394 (2013) 515-521, http://dx.doi.org/10.1016/j.jcis.2012.12.034.

[70] Z.X. Song, L.T. Yin, Q.L. Zhang, P. Ning, Y.K. Duan, J. Wang, X. Liu, K.X. Long, Z.Z. Huang, Relationship between the WO_3 states and reaction pathway over CeO_2-ZrO_2-WO_3 catalysts for selective catalytic reduction of NO with NH_3, Mol. Catal. 437 (2017) 95-104, http://dx.doi.org/10.1016/j.mcat.2017.04.033.

[71] J.J. Zou, S. Impeng, F.L. Wang, T.W. Lan, L.L. Wang, P.L. Wang, D.S. Zhang, Compensation or Aggravation:

948 Pb and SO_2 Copoisoning Effects over Ceria-Based Catalysts for NO_x Reduction, Environ. Sci. Technol. 56
949 (2022) 13368-13378, https://doi.org/10.1021/acs.est.2c03653.
950 [72] A. Younis, D.W. Chu, Y.V. Kaneti, S.A. Li, Tuning the surface oxygen concentration of {111} surrounded ceria
951 nanocrystals for enhanced photocatalytic activities, Nanoscale 8 (2016) 378,
952 https://doi.org/10.1039/C5NR06588G.
953 [73] W.Y Song, B.Z Zhu, Y.L. Sun, C.Y. Xie, Effect of calcination atmosphere on low-temperature denitrification
954 of citric acid sol-gel iron oxide catalyst, Clean. Coal. Technol. 26 (2020) 56-63, https://10.13226/j.issn.1006-
955 6772.IF20080602.
956 [74] L. Huang, Y.W. Yue, Y.H. Zong, J.K. Li, Y.B. Gao, H. Wang, P. Han, Effect of impregnation sequence of
957 vanadium and molybdenum on the Na resistance of de-NO_x catalyst, Clean. Coal. Technol. 29 (2023) 74-79,
958 https://10.13226/j.issn.1006-6772.22051703.
959 [75] T. Yi, Y.B. Zhang, J.W. Li, X.G. Yang, Promotional effect of H_3PO_4 on ceria catalyst for selective catalytic
960 reduction of NO by NH_3, Chinese. J. Catal 37 (2016) 300-307, https://doi.org/10.1016/S1872-2067(15)60977-
961 9.
962 [76] L. Zhang, L.L. Li, Y. Cao, X.J. Yao, C.Y. Ge, F. Gao, Y. Deng, C.J. Tang, L. Dong, Getting insight into the
963 influence of SO_2 on TiO_2/CeO_2 for the selective catalytic reduction of NO by NH_3, Appl. Catal. B: Environ
964 165 (2015) 589-598, http://dx.doi.org/10.1016/j.apcatb.2014.10.029.
965 [77] Z.X. Song, Q.L. Zhang, P. Ning, X. Liu, J. Fan, Z.Z. Huang, Introduction manner of sulfate acid for improving
966 the performance of SO_4^{2-}/CeO_2 on selective catalytic reduction of NO by NH_3, J. Rare Earths 34 (2016) 667,
967 https://doi.org/10.1016/S1002-0721(16)60077-7.
968 [78] S. Hoffmann, M. Schmidt, S. Scharsach, R. Kniep, TG-MS of air-sensitive compounds in argon, Thermochim.
969 Acta. 527 (2012) 204-210, https://doi.org/10.1016/j.tca.2011.10.024.

970 [79] G. Zelenková, V. Slovák, Decomposition of ammonium salts by quantitative TG-MS, J. Therm Anal Calorim
971 147 (2022) 15059-15068, https://doi.org/10.1007/s10973-022-11747-0.
972 [80] J.J. Liu, X.Y. Shi, Z.H. Lv, Y.B. Yu, H. He, Ceria-tungsten-tin oxide catalysts with superior regeneration
973 capacity after sulfur poisoning for NH_3-SCR process, Catal. Sci. Technol. 12 (2022) 2471,
974 https://doi.org/10.1039/D2CY00036A.
975 [81] L. Ma, C.Y. Seo, M. Nahata, X.Y. Chen, J.H. Li, J.W. Schwank, Shape dependence and sulfate promotion of
976 CeO_2 for selective catalytic reduction of NO_x with NH_3, Appl. Catal. B: Environ 232 (2018) 246-259,
977 https://doi.org/10.1016/j.apcatb.2018.03.065.
978 [82] J. Yang, S. Ren, T.S. Zhang, Z.H. Su, H.M. Long, M. Kong, L. Yao, Iron doped effects on active sites formation
979 over activated carbon supported Mn-Ce oxide catalysts for low-temperature SCR of NO, Chem. Eng. J. 379
980 (2020) 122398, https://doi.org/10.1016/j.cej.2019.122398.
981 [83] J. Arfaoui, A. Ghorbel, C. Petitto, G. Delahay, Effect of acidic components (SO_4^{2-} and WO_3) on the surface
982 acidity, redox ability and NH_3-SCR activity of new CeO_2-TiO_2 nanoporous aerogel catalysts: A comparative
983 study, Inorg. Chem. Commun. 140 (2022) 109494, https://doi.org/10.1016/j.inoche.2022.109494.
984 [84] S.J. Yang, Y.F. Guo, H.Z. Chang, L. Ma, Y. Peng, Z. Qu, N.Q. Yan, C.Z. Wang, J.H. Li, Novel effect of SO_2
985 on the SCR reaction over CeO_2: Mechanism and significance, Appl. Catal. B: Environ 136-137 (2013) 19-28,
986 http://dx.doi.org/10.1016/j.apcatb.2013.01.028.
987 [85] P. Zhang, W.G. Pan, R.T. Guo, X.B. Zhu, J. Liu, L. Qin, X.L. She, The Mo modified Ce/TiO_2 catalyst for
988 simultaneous Hg^0 oxidation and NO reduction, J. Energy Inst 92 (2019) 1313-1328,
989 https://doi.org/10.1016/j.joei.2018.10.003.
990 [86] J. Li, F. Zhou, Z.B. Xiong, Y.P. Du, Q.G. Yang, W. Wang, W. Lu, Promotional Effect of Zirconium Doping on
991 the NH_3-SCR Activity of CeO_2 and CeO_2-TA Modified by Thiourea: A Comparative Study. Chemcatchem. 15

992 (2023) e202201578, https://doi.org/10.1002/cctc.202201578.

993 [87] G.Y. Zhou, P. Maitarad, P.L. Wang, L.P. Han, T.T. Yan, H.R. Li, J.P. Zhang, L.Y. shi, D.S. Zhang, Alkali-
994 Resistant NO_x Reduction over SCR Catalysts via Boosting NH_3 Adsorption Rates by In Situ Constructing the
995 Sacrificed Sites. Environ. Sci. Technol. 54 (2020) 13314−13321, https://dx.doi.org/10.1021/acs.est.0c04536.

996 [88] H.Q. Wang, S. Gao, F.X. Yu, Y. Liu, X.L. Wen, Z.B. Wu, Effective Way to Control the Performance of a Ceria-
997 Based $DeNO_x$ Catalyst with Improved Alkali Resistance: Acid−Base Adjusting. J. Phys. Chem. C 119 (2015)
998 15077-15084, http://dx.doi.org/10.1021/acs.jpcc.5b00793.

999 [89] M.N. Khan, L.P. Han, P.L. Wang, J.B. He, B. Yang, T.T. Yan, L.Y. Shi, D.S. Zhang, SO_2-tolerant NO_x reduction
1000 over ceria-based catalysts: Shielding effects of hollandite Mn-Ti oxides. Chem. Eng. J. 397 (2020) 125535,
1001 https://doi.org/10.1016/j.cej.2020.125535.

1002 [90] Q. Xie, D.Q. An, L.S. Zhou, T.Z. Li, Z.H. Hu, M.H. Chen, M.L. Ma, L. Zhang, J.F. Sun, L. Dong, Deactivation
1003 induced by metal sulfate over $MnCeO_x$ catalyst in NH_3-SCR reaction at low temperature. J. Rare. Earth. (2023),
1004 https://doi.org/10.1016/j.jre.2023.07.004.

1005 [91] Y.F. Xu, X.D. Wu, Q.W. Lin, J.F. Hu, R. Ran, D. Weng, SO_2 promoted V_2O_5-MoO_3/TiO_2 catalyst for NH_3-
1006 SCR of NO_x at low temperatures. Appl. Catal. A-Gen. 570 (2019) 42-50,
1007 https://doi.org/10.1016/j.apcata.2018.10.040.

1008 [92] A.C. Zhang, W.B. Xing, Z.H. Zhang, F.M. Meng, Z.C. Liu, J. Xiang, L.S. Sun, Promotional effect of SO_2 on
1009 CeO_2-TiO_2 material for elemental mercury removal at low temperature. Atmos. Pollut. Res. 7 (2016) 895-902,
1010 http://dx.doi.org/10.1016/j.apr.2016.05.003.

1011 [93] M.D. Lane, Mid-infrared emission spectroscopy of sulfate and sulfate-bearing minerals. Am. Mineral. 92
1012 (2007) 1-18, https://doi.org/10.2138/am.2007.2170.

1013 [94] D.Q. An, S. Yang, W.X. Zou, J.F. Sun, W. Tan, J.W. Ji, Q. Tong, C.Z. Sun, D. Li, L. Dong, Unraveling the SO_2

Poisoning Effect over the Lifetime of MeO_x (Me=Ce, Fe, Mn) Catalysts in Low-Temperature NH_3-SCR: Interaction of Reaction Atmosphere with Surface Species. J. Phys. Chem. C 126 (2022) 12168-12177, https://doi.org/10.1021/acs.jpcc.2c02233.

[95] G.H. Kim, S. Jeong, I. Lee, M.A. Hanif, M.A. Islam, K.P. Sapkota, J.R. Hahn, Role of Electronic Structures and Dispersion Interactions in Adsorption Selectivity of Pyrimidine Molecules with a Si (5 5 12) Surface, J. Phys. Chem. C 123 (2019) 19506-19512, https://doi.org/10.1021/acs.jpcc.9b03520.

[96] W.G. Schmidt, K. Seino, M. Preuss, A. Hermann, F. Ortmann , F. Bechstedt, Organic molecule adsorption on solid surfaces: chemical bonding, mutual polarisation and dispersion interaction, Appl. Phys. A 85 (2006) 387-397, https://doi.org/10.1007/s00339-006-3691-0.

[97] R.A. van Santen, I. Trancab, How molecular is the chemisorptive bond? Phys. Chem. Chem. Phys. 18 (2016) 20868-20894, https://doi.org/10.1039/C6CP01394E.

[98] L. Zhang, X.Y. Yang, L. Zhang, H. Shu, Y. Jia, L.B. Qi, Y.Z. Han, R. Wang, Preparation of nano-hollow sphere hydrolytic catalyst and study on its COS removal performance, J. Nanopart. Res. 24 (2022) 268, https://doi.org/10.1007/s11051-022-05641-x.

[99] R.H. Sui, C.B. Lavery, C.E. Deering, R. Prinsloo, D. Li, N. Chou, K.L. Lesage, R.A. Marriott, Improved carbon disulfide conversion: Modification of an alumina Claus catalyst by deposition of transition metal oxides, Appl. Catal. A: General 604 (2020) 117773, https://doi.org/10.1016/j.apcata.2020.117773.